On Optical-Signal-to-Noise Ratio and Polarization-Mode-Dispersion Monitoring in Optical Networks

MAN-HONG CHEUNG

A Thesis Submitted in Partial Fulfillment
of the Requirements for the Degree of
Master of Philosophy

in

Information Engineering

July 2004

Acknowledgement

It was his tenacious research principle "Everything has tradeoff" that reminded me of the futility to hunt for any perfect scheme. Yet for several traumatic months I just wandered in the laboratory without any good idea. Stuck, I was given important directions, guidance, and comments from him. I started to evaluate previous schemes with a conscientious mind to look at both strengths and weaknesses. I went deeper and deeper in my analysis, and my new ideas suddenly surfaced and flooded. Thanks must be given to my supervisor, Prof. Lian-Kuan Chen. His apposite training helped me think freely as if bondage was broken. He has additionally taught me to have high-principled research ethics and the right research attitude, sometimes virtuous behavior as well.

Many thanks are also due to Prof. Calvin Chan and Prof. Chinlon Lin who enlightened me with their in-depth knowledge, advice, and discussion. They encouraged me with praise and strengthened me with challenges so that I found my problem-solving abilities had been greatly enhanced.

In addition, I am indebted to many talents who gave me freely of their knowledge, expertise, time, and effort to make my dissertation possible. They include Mr. Vincent Hung, Mr. Kit Chan, Mr. Guo-Wei Lu, Ms. Yu Zhang, Mr. Zhao-Xin Wang, Ms. Yi Yang, Mr. Jimmy Chan, Mr. Jordan Tse, Mr. Scott Tam, Mr. Jam Ku, Mr. Chi-Man Lee, Mr. Ning Deng, Mr. Jian Zhao, Mr. Siu-Sun Pun, Mr. Siu-Ting Ho, and Mr. Xiao-Feng Sun. Without their generous support my research would have never borne fruit.

Finally, I am grateful to my parents for their tender love and resolute support. I must also thank my beloved God. What else can I say when I see this wonderful optical world created? This thesis is dedicated to God.

Abstract

Optical signal-to-noise ratio (OSNR) and polarization-mode-dispersion (PMD) are two important parameters to be monitored in future optical networks for proper network management. This thesis is devoted to the evaluation of the accuracy of reported in-band polarization-assisted OSNR monitoring schemes as well as the proposal of new, accurate OSNR and PMD monitoring techniques.

The first part of the thesis presents our theoretical calculations and experimental results on the robustness of three reported in-band polarization-assisted OSNR monitoring schemes, namely, polarization-nulling, DOP-based OSNR monitoring, and orthogonal delayed-homodyne method against PMD for different pulse widths. Our detailed quantification of the monitoring errors helps identify system conditions which necessitate improvements on these monitoring schemes.

The second part of the thesis elucidates a new, simple, and PMD-insensitive OSNR monitoring scheme based on polarization-nulling with off-center narrowband filtering. Amelioration on the PMD robustness is demonstrated with both theoretical calculations and experiments. The effects of filter position, filter bandwidth, and filter detuning will also be investigated and discussed.

The final part of the thesis demonstrates two simultaneous OSNR and PMD monitoring schemes using polarization techniques. The first one employs enhanced RF spectral analysis while the second one is based upon degree-of-polarization (DOP). Experimental results demonstrate their feasibility to provide a more comprehensive monitoring picture to network operators compared with single parameter monitoring modules.

摘要

在未來光網路的網路管理中，光信噪比(OSNR)和偏振模色散(PMD)是兩個重要的監測參數。本論文將評估已報導的偏振輔助帶內光信噪比監測方案的準確性，並提出新而準確的光信噪比和偏振模色散檢測技術。

本論文第一部分主要就已報導的三種偏振輔助帶內光信噪比監測方案對偏振模色散的魯棒性進行理論和實驗分析。這三種方案包括基於偏振歸零(Polarization-Nulling)、偏振度(DOP)、以及正交延遲零拍技術(Orthogonal-Delayed Homodyne Method)的光信噪比監測方案。我們利用不同脈衝濶度進行了詳細的監測誤差定量分析，這將有助於決定系統是否需要進一步改進監測方案。

本論文的第二部分闡述了一種全新、簡單、基於偏振歸零及偏移窄濾波器的光信噪比監測方案。理論計算和實驗均表明，這種改進的方案可使抗偏振模色散的魯棒性大爲提高，而論文亦同時就窄濾波器的位置、頻寬及漂移作出了分析和討論。

本論文的最後一部分主要用實驗展示了兩種基於偏振技術的光信噪比和偏振模色散同時監測的方案。第一種方案主要採用改進的射頻譜分析方法，第二種方案基於偏振度的分析。實驗結果表明，比較單一的監測方案，這種同時監測的方案給網路供應商提供了更爲全面的監測手段。

Table of Contents

List of Figures

List of Tables

Chapter 1 Introduction

1.1 Drivers for Advanced Optical Performance Monitoring (OPM) Techniques

In recent years, the proliferation of Internet traffic has triggered the rapid development of optical networks. Such development generally centers around three important elements that make up the service provider's network: (i) the network infrastructure hardware, (ii) the applications and services that utilize the network infrastructure, and (iii) the monitoring and management systems [1]. It is perhaps the last element that is capturing the least attention because it is typically not viewed as the leading edge technology. Nonetheless, one cannot deny that performance monitoring systems are crucial pieces of the network puzzle because it is they who help prevent and identify network degradation and failure that would otherwise translate to colossal financial loss for both service providers and customers.

Performance monitoring (PM) of traditional SONET/SDH (synchronous optical network/synchronous digital hierarchy) networks typically require optical/electrical/optical (O/E/O) conversion in the data path. Service providers may determine (i) the bit/block error rates (BERs) at SONET line terminating elements (LTEs) by a protocol-dependent method called bit interleaved parity-8 (BIP-8) [1]-[4], (ii) Q-factor from bits interleaved within the SONET frame, and/or (iii) simple loss of signal (LOS) using power monitoring fiber taps. The signal-to-noise (SNR) degradation and distortion are usually pre-determined by measuring the

characteristics of active and passive optical components in advance [5]. As a result the efficacy of the PM metrics rests on the assumptions that the networks are opaque and static.

Future optical networks, however, have a number of characteristics that drive the need for a new paradigm of more advanced monitoring techniques called optical performance monitoring (OPM) [5]-[10]:

Firstly, future optical networks will be *all-optical*, meaning that routing will be done entirely in the optical domain and the O/E/O conversion points will be eliminated. The monitoring paradigm thus shifts from the O/E/O regeneration approach to optical power tap approach, in which a portion of optical power is removed from the fiber and converted to an electronic signal for non-intrusive PM after possible optical signal processing (Fig. 1.1).

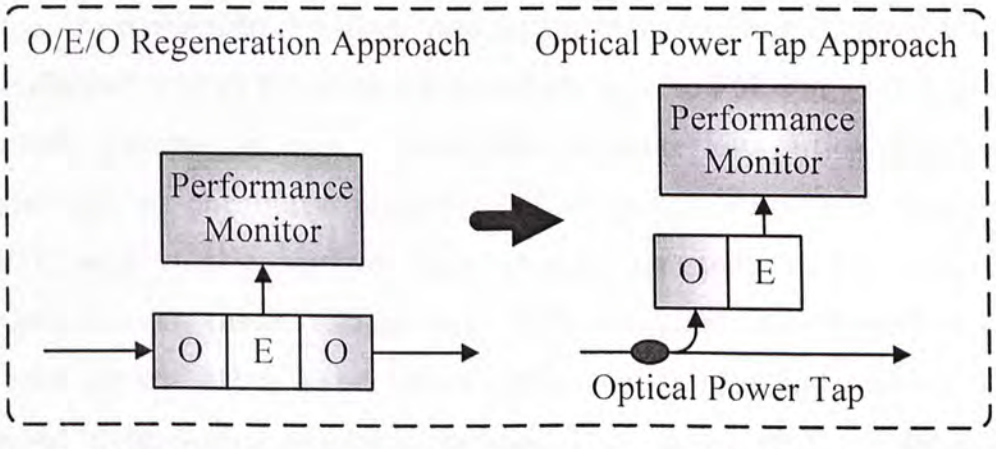

Figure 1.1: Performance monitoring migrates from the O/E/O regeneration approach to the optical power tap approach

Secondly, future optical networks will be *transparent*, meaning that they can accommodate signals with different protocols including SDH/SONET, Gigabit Ethernet, ATM, IP over WDM and a plurality of

others that are once confined within the boundaries of the enterprise network environment. The monitoring unit therefore may not have prior knowledge about the protocol, format, and data-rate of the signal, thus new non-intrusive OPM techniques that do not need to decode the overhead information are required.

Thirdly, future optical networks will be *dynamically reconfigurable*, meaning the signals will traverse different complex paths consisting of different fibers, amplifiers, optical add/drop multiplexers (OADM), optical cross-connects (OXC), and plenty of other network elements. The monitoring schemes should therefore be insensitive to signal origins and its transport path history, be on a per-channel basis, and tie closely with adaptive compensation techniques to provide optimum system conditions in a dynamic manner.

Last but not least, future optical networks will have *higher data rates, increased wavelength densities, and longer transmission distance*. Each of these characteristics presents unique challenges to PM. For example, high data-rate systems are highly susceptible to deleterious optical fiber-based effects such as chromatic dispersion (CD), polarization-mode-dispersion (PMD), and nonlinearities, thus monitoring techniques with high sensitivities to these effects are desired. Tight wavelength-spacing systems, on the other hand, cause overlap of falling and trailing edges between neighboring signal channels. This may create problems for spectrum-interpolated OSNR monitoring and demand more accurate wavelength monitoring. Finally, in long-distance transmission systems, impairments will be accumulated from more unknown places, making fault localization more difficult. All these create an urgent need for new OPM technologies and strategies that can effectively meet the above challenges.

1.2 OPM: Definition and Significance

Owing to its importance, the topic of OPM has been hotly discussed in literature and the buzzword itself has also taken on multiple definitions [11]-[17]: On a broad sense, OPM may simply mean physical layer monitoring of the optical signal quality [17]. A somewhat more restrictive sense of OPM would be an approach to characterize the channel parameters without prior knowledge of origin, transport history, format and data content at arbitrary points of the networks [18]. OPM is not just hype; it does deliver on its promises to a large extent. It serves a number of important network functions that spans at least the following:

- *Active time-varying distortion monitoring and compensation* – The performance monitors can be used to provide direct feedback for adaptive compensators. Some examples include PMD compensation, distortion compensation, and dynamic gain equalization (DGE) for amplifiers [18], [24]

- *Fault forecasting, detection, localization, isolation, and resilience mechanism activation* – The performance monitors can be used to anticipate major degradations of components like erbium-doped fiber amplifiers (EDFA), OADM, and OXC, as well as changes in working conditions after the initial service rollout. Protection and restoration mechanisms will be triggered within timing limits when necessary [17]-[18].

- *New network functionality such as intelligent path provisioning and traffic routing based on OPM* – For example, high capacity and priority traffic can be dynamically tuned to high-performance optical

channels. In addition, channel commissioning and topology discovery can also be based on OPM [11]-[12], [24].

- *Signal quality characterization for quality of service (QoS) assurance and service level agreement (SLA) fulfillment* – Under the terms of SLA, the service providers guarantee a measurable QoS to customers. These QoS measures may be in terms of committed network availability, provisioning time, target repair time and procedures and a host of others. If the conditions in the agreement are violated, the carriers will typically provide a rebate to the customers. OPM-enabled QoS measurements will present new opportunities for revenue and competitive differentiation for the service providers [8], [17].

1.3 The Broad Spectrum of OPM

Today the deployment of OPM is still in its embryonic stage. Current mass deployed performance monitors typically provide information on parameters including (i) aggregate signal power, (ii) individual component's health status such as amplifier pump laser power or temperature controller limits, and (iii) individual channel power, presence, wavelength, and/or spectrum-interpolated optical signal-to-noise ratio (OSNR) [17]-[18]. An illustration of a long-haul network with OPM is shown in Fig. 1.2. These parameters, however, represent only a small part of the overall monitoring picture. As networks continue to evolve to higher-speed with more channel counts to longer distance, more advanced OPM is necessary. Fig. 1.3 shows the broad spectrum of OPM with the plethora of parameters to be monitored classified into three categories: signal loss, signal alignment, and signal quality [20].

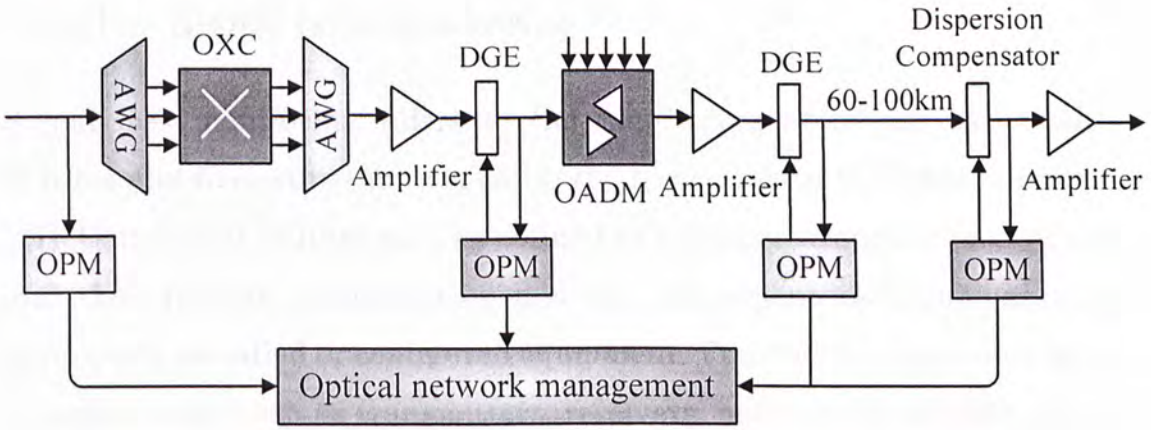

Figure 1.2: A long-haul network with OPM

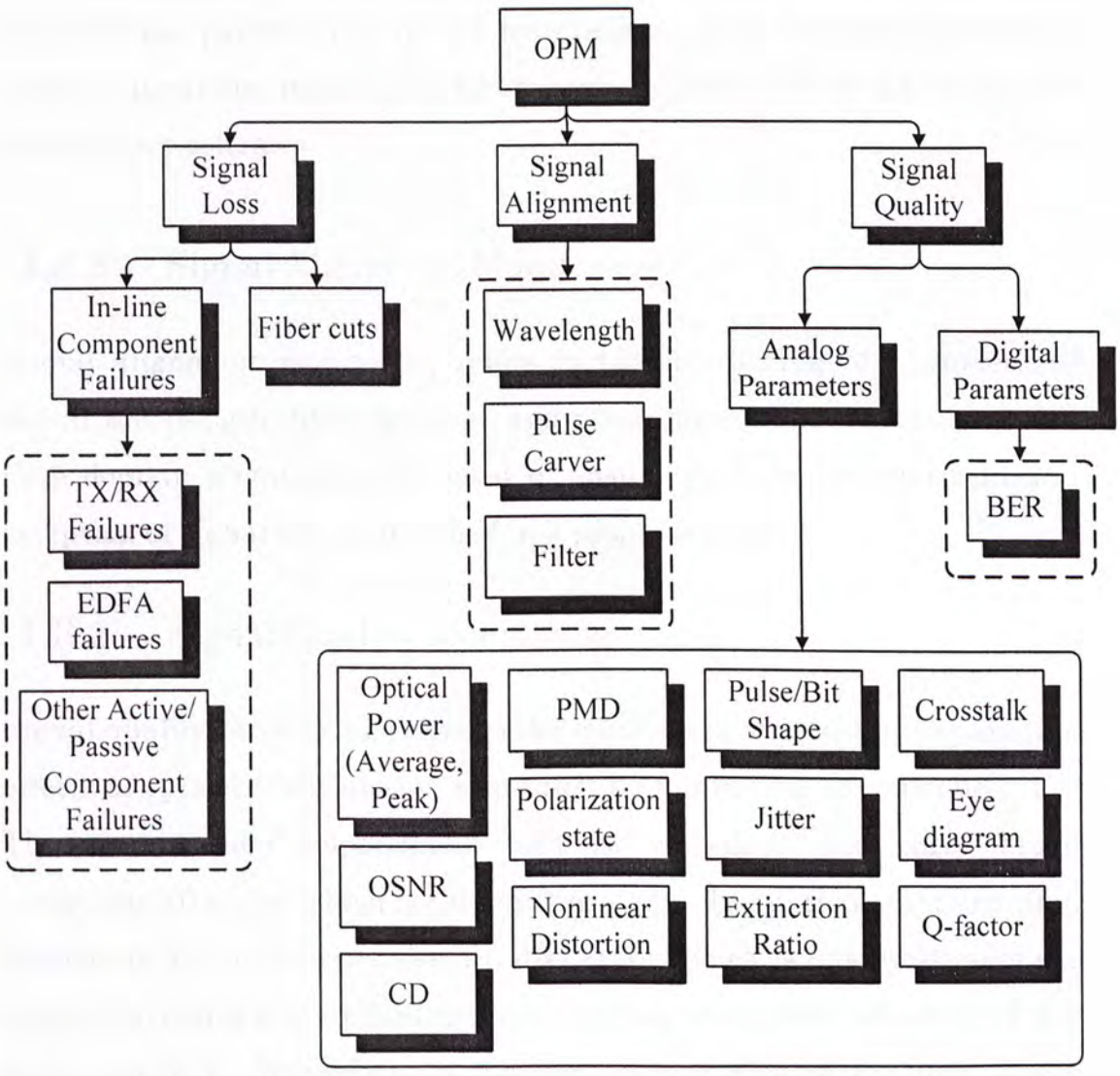

Figure 1.3: The broad spectrum of OPM

1.3.1 Signal Loss Monitoring

Signal loss monitoring refers to the monitoring of in-line component failures and fiber cuts that can cause the power loss of the whole channel [17]. Component failures may be defined as a change in opacity (e.g. >2 dB) and they include individual or multiple component malfunctions and improperly installed or configured equipment. The faulty components may be active ones, such as transmitters, receivers, and optical amplifiers, i.e. pump laser failure, or passive ones, such as arrayed-waveguide grating (AWG). On the other hand, fiber cuts are damage to the network fibers due to accidents, periodic repair and maintenance, and deliberate malicious attack. Signal loss monitoring schemes are typically referred to as optical surveillance schemes.

1.3.2 Signal Alignment Monitoring

Signal alignment monitoring refers to the monitoring of alignment of signal wavelength, filter position, and pulse carver. These frequency and time domain alignments are used to ensure that the transmission and reception of signal are maintained in a proper condition.

1.3.3 Signal Quality Monitoring

Signal quality monitoring refers to the monitoring of a host of disparaging effects of optical transmission that must be minimized or controlled [17]. The transmission impairments can be classified into three broad categories: (i) noise, which is the random signal fluctuations that are often treated as a Gaussian process, (ii) distortion, which is modification of the signal waveform due to nonlinearities or fiber dispersion effects, and (iii) jitter, which is fluctuation in the time registration of the bits. These

notable transmission impairments include amplifier noise, amplifier distortion and transients, CD, PMD, polarization dependent gain (PDG), polarization dependent loss (PDL), fiber nonlinearity induced distortion and crosstalk including self-phase modulation (SPM), cross-phase modulation (XPM), four-wave mixing (FWM), stimulated Rayleigh scattering (SRS), and stimulated Brillouin scattering (SBS), timing jitter, interference effects (MPI), pump laser RIN transfer, optical filter distortion, and linear crosstalk. In response to these impairments, OPM has been vigorously pursued in laboratories to provide the following physical layer measurements [5], [17]:

1) average power (per wavelength or aggregate);
2) peak power;
3) optical signal-to-noise ratio;
4) chromatic dispersion;
5) polarization-mode dispersion (first and higher order);
6) polarization state;
7) nonlinear distortion;
8) pulse/bit shape;
9) jitter;
10) extinction ratio;
11) crosstalk;
12) eye diagram;
13) Q-factor;
14) BER;

The above list is, however, by no means exhaustive as new performance metrics always emerge as optical networking technologies advance.

1.4 Classification of OPM Techniques

As listed in previous section, there are multifarious parameters to be monitored in the optical networks. Depending on these parameters, OPM techniques can be classified in different ways detailed in the following subsections:

1.4.1 Time Domain vs. Frequency Domain Monitoring

Time domain monitoring gathers time-varying information including eye diagram, intensity, pulse shape, and time-varying statistics like power, polarization state, jitter, and wavelength. Frequency domain monitoring gathers spectral information and can be further broken down into optical spectral and RF spectral measurements. The optical spectrum is conveniently measured using highly sensitive optical techniques and it can provide channel power, wavelength, bit-rate, format, optical noise, RZ clock, and spectral phase information. The RF spectrum measures the spectrum of the signal that is encoded on the optical carrier (assuming intensity on-off keying (OOK) modulation) and it can provide information about electrical noise, RZ clock, and low/high frequency tones that are commonly used as dispersion indicators [17].

1.4.2 Analog Parameter vs. Digital Parameter Monitoring

Another way to classify OPM is to differentiate it between analog and digital parameter monitoring. Analog measurement techniques treat the optical signal as an analog waveform and attempt to measure specific characteristics of this waveform. Examples of analog parameters include distortion, OSNR and Q-factor. Digital measurement techniques, on the other hand, typically rely on looking into the bit pattern and counting the

block/bit error rates – blocks in a digital form are monitored by an error detection code (EDC) which allows the detection of an erroneous block with a certain probability. An example of digital parameter monitoring is the Digital Wrapper scheme. It encapsulates multi-protocol data packets into SONET-like frames and uses BIP-8 as the EDC code to calculate the errors for each frame. In ITU-T G.709, it is agreed that applying BIP within the Digital Wrapper frame is sufficient for monitoring channels in the optical domain [7].

	Analog parameter	Digital parameter
Advantages	Faster, simpler, more economical	More accurate and sensitive
Disadvantages	Less accurate and sensitive	More expensive and slower, needs standardization
Main uses	Fault localization, fault identification, performance optimization	End-to-end performance guarantee, resilience mechanism activation, SLA verification
Typical locations	Nodes and amplifiers in optical layer	Digital equipment at ends of optical paths

Table 1.1: Comparison of analog and digital parameter monitoring

A comparison of analog and digital parameter monitoring is made in Table 1.1. In general, analog techniques are less accurate, but are faster, simpler, and relatively less expensive for performance assessment, particularly for troubleshooting [23]. In contrast, digital techniques are slower and more expensive, but can guarantee in-service reliable measurements of the end-to-end performance of an optical channel.

Analog and digital monitoring techniques will therefore play complementary role and both techniques appear to have a promising future in next-generation optical networks.

1.4.3 Three-Tier OPM

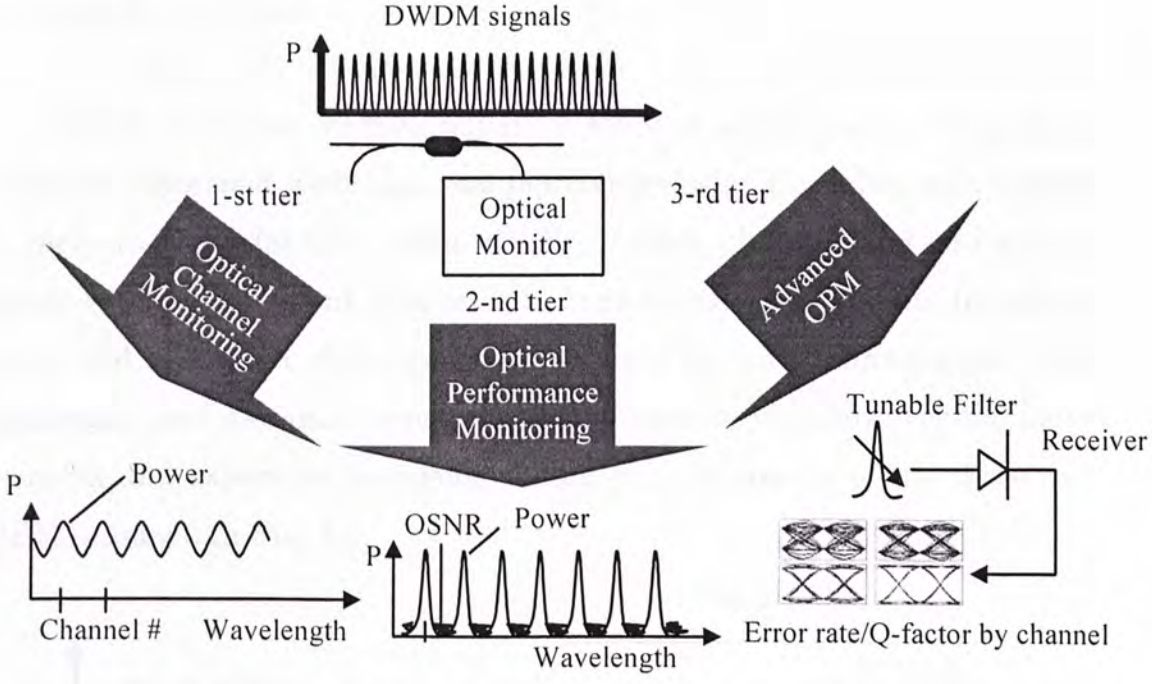

Figure 1.4: Three-tier OPM (Adapted from [21])

A third way to break down OPM is to divide it into three different tiers (Fig. 1.4) [21]. On the first tier, we have optical channel monitoring (OCM), which is concerned with low-end per-channel power and wavelength monitoring. An OCM monitor is usually implemented by a filter or a grating to separate the wavelength components, plus a detector array to convert the optical signal into electrical signal for further processing [22]. The main use of OCM is in dynamic gain equalization for amplifiers. However, it also finds use in applications such as fault isolation and channel routing supervision.

On the second tier, we have basic optical performance monitoring (OPM), which provides per-channel power and wavelength monitoring as well as spectral OSNR monitoring. The information obtained enables service providers to have a tighter control over the DWDM wavelengths in order to accommodate higher spectral efficiency. OPM is slightly costly than OCM and so the monitors should be placed in a less massive way through the networks.

On the third tier, we have advanced OPM or signal quality monitoring, which is concerned with high-end per-channel signal quality monitoring. It measures the bit-error ratio (BER) of each channel and provides a quantitative assessment of a multitude of signal impairments including noise and distortion. Advanced OPM is used in fault management, QoS assurance, and dynamic dispersion compensation. It is however the most complex and expensive technology category. A summary of the three-tier OPM is shown in Fig. 1.5.

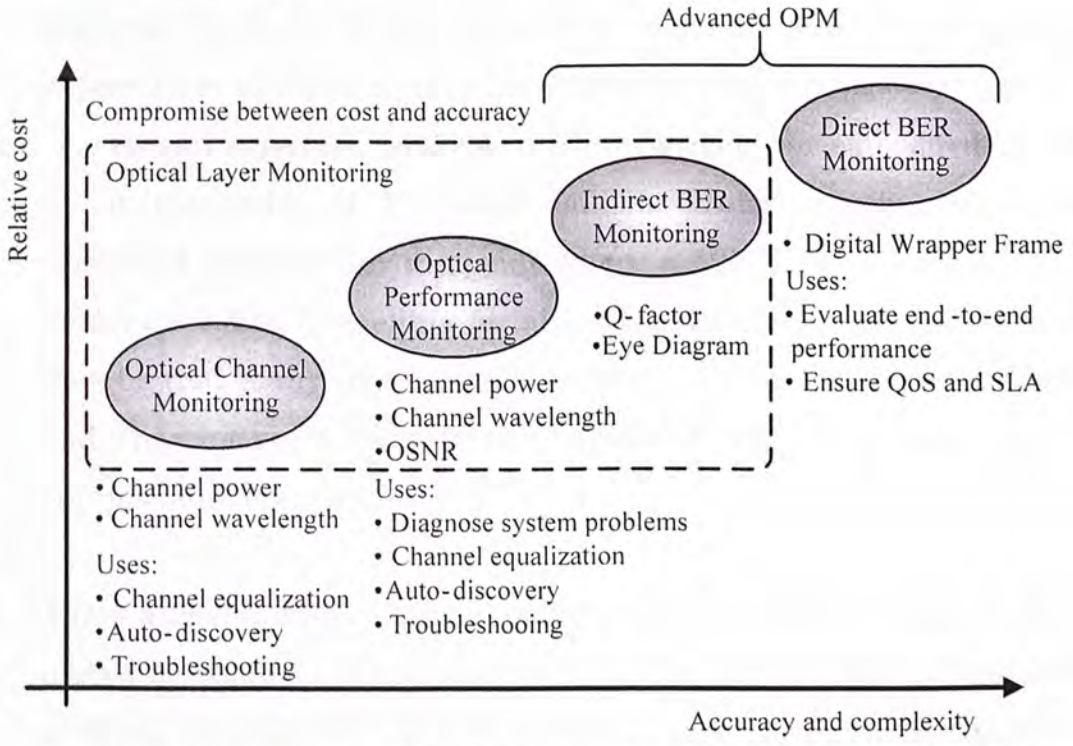

Figure 1.5: Summary of the three-tier OPM (Adapted from Ref[7])

1.5 Challenges and Requirements of OPM Techniques

To be effective, any monitoring technique should satisfy some general requirements [6], [15]-[16]. These can be classified into technical requirements, commercial requirements, and value-added options.

- *Technical requirements* – From the technical perspective, desirable OPM options should have signal degradation discovery capability, transparency in terms of bit rate, modulation format, and protocol, non-intrusiveness (in-service measurement), high update speed, accuracy, reliability, and stability.

- *Commercial requirements* – From the commercial perspective, desirable OPM options should have low production cost, low power consumption, compactness, simplicity, and interoperability between different vendors. Cost is the major concern here as the capital expense due to OPM must be recovered through savings over time in operational expenses. In 2004, the total market for embedded OPMs is on the order of US$10-20 million. Unfortunately, price has continued unabated to the point where a 100-GHz-capable OPM in moderate volume is selling for about US$3,000 [24]. A positive sign may be that many recent optical technologies such as tunable filters and spectrometers have become available and made many OPM options more economical [17].

- *Value-added options* – An increasing focus of OPM development is placed on comprehensiveness (whether the OPM option can monitor multiple parameters simultaneously), fault localization capability

(whether the OPM option can locate the source of degradation), and scalability (whether the OPM option can adapt to high data-rate systems).

Besides, OPM deployment also faces some other important challenges:

- *Standards and interoperability* – Since there are no large incumbent suppliers of OPMs, the industry does not quickly coalesce around a single standard interface. Thus, aggressive and concrete measures to standardize OPM are needed before it is too late or too expensive to retrofit proprietary OPM methods.

- *Inter-layer coordination* – Interactions between OPM and higher-level element management systems (EMS) and network management system (NMS) become a critical issue. Questions arise such as what information should be passed around the network in order to keep the network management scalable. These aspects have been addressed in recent OPM drafts within the IETF [26].

- *Network design issue* – Concern centers around where we should put the OPM modules and how much monitoring functions are needed. One consideration for the placement of OPM modules, for example, is whether it should be centralized or distributed [6]. Centralized OPM collects information from other segments of optical transmission links and processes the information at a strategic point. It facilitates centralized decision-making and fault localization. Distributed OPM can collect and process information easily, but as the number of monitoring modules increases, cost and means to integrate the OPM with the in-line components are of concern. Another more complicated problem is how to place the monitors with minimum redundancy. This monitor placement problem is formulated as an optimization problem

in [25] and is shown to be NP-complete. It is expected that more research in this area will be carried out.

1.6 Thesis Outline

In this thesis, we address two of the most challenging problems, OSNR and PMD monitoring, in OPM. The thesis is organized as follows:

Chapter 1: This chapter introduces the background of OPM ranging from its drivers, definition, significance, classification, requirements, and challenges.

Chapter 2: This chapter narrows down to OSNR and PMD monitoring techniques with their classification and review presented.

Chapter 3: This chapter reports on our comprehensive study on the PMD robustness of three reported in-band polarization-assisted OSNR monitoring schemes.

Chapter 4: This chapter introduces our newly proposed PMD-insensitive OSNR monitoring scheme. The effectiveness of this scheme as well as the effects of filter position, filter bandwidth, and filter detuning will be investigated.

Chapter 5: This chapter demonstrates the feasibility of two simultaneous OSNR and PMD monitoring methods using enhanced RF spectral analysis and enhanced DOP monitoring.

Chapter 6: This chapter summarizes the thesis and discusses the possible future work.

Chapter 2 Review on OSNR and PMD Monitoring

2.1 Optical Signal-to-Noise-Ratio (OSNR) Monitoring

According to TIA-EIA-526-19 standard [27], the definition of OSNR is $10\log(P_{sig}/P_{ase})$, where P_{sig} is the signal power measured with a filter with 3-dB bandwidth large enough to cover the whole signal spectrum, i.e. 0.2 nm for 10-Gb/s NRZ signal, and P_{ase} is noise measured with a filter of known noise equivalent bandwidth (NEB). N is typically referenced to 0.1-nm NEB, although a 1-nm NEB is sometimes used (Fig. 2.1).

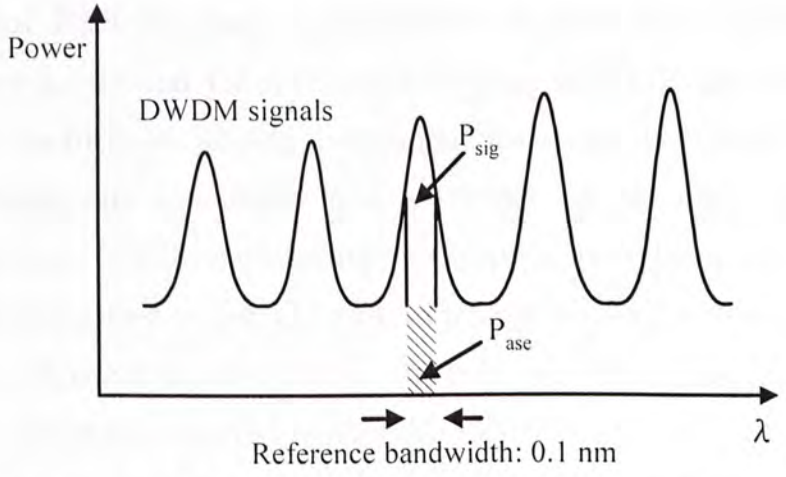

Figure 2.1: OSNR measurement in DWDM system

OSNR is important because it suggests a degree of impairment when the optical signal is carried in links with optical amplifiers. Optical amplifiers introduce additional impairments because the amplified spontaneous emission (ASE) noise will contribute electrical noise after

O/E conversion in the receivers. In practice, the use of amplifiers will improve the signal as the increase in the signal amplitude will help overcome the noise generated in the receiver's front end. However, the optical background noise that accompanies the desired optical signal will be amplified along with signal as well. Consequently, the OSNR will tend to degrade as it passes through the transmission system [28]. One of the consequences of having a low OSNR is that no matter how strong the signal presented to a good receiver, there will be errors associated with the presence of the ASE. Thus, there exists a minimum acceptable OSNR for a given BER [29].

As a result of the above property, OSNR has been vigorously pursued as an important analog performance metric for (i) link setup, control, and optimization, such as tuning a dynamic gain equalizer [18], (ii) in-service signal quality characterization for QoS assurance [7], (iii) correlation with end-terminal BER for fault management purposes [30], and (iv) path performance prediction for intelligent routing [12][17]. Desirable OSNR monitoring techniques should be simple, accurate, low-cost, with large dynamic range and sensitivity, and requiring low monitoring power. To date, numerous OSNR monitoring techniques have been proposed and they can be classified as out-of-band, in which the ASE noise is measured outside the channel bandwidth, or in-band, in which the ASE noise is measured within the channel bandwidth [6].

2.2 Out-of-band OSNR Monitoring Techniques

2.2.1 Optical Spectral Analysis

One of the most commonly used techniques for out-of-band OSNR monitoring is optical spectral analysis (OSA). A small portion (~1-5%) of

the transmitted optical signal is tapped and sent to an optical spectrum analyzer. The ASE noise spectrum lying between the channels can be used to derive an estimate of the in-band ASE noise by linear interpolation. However, there are two general cases in which spectral monitoring becomes problematic: dense WDM channel packing and dynamic reconfigurable networks [31]. For networks with dense WDM channel spacing, such as 10 Gb/s RZ modulated channels on a 50-GHz ITU grid, there is insufficient spectrum available for monitoring between the channels and the OSNR measurement is hindered by crosstalk from adjacent channels. For dynamic reconfigurable networks, each channel may traverse a different route with a different number of Erbium-doped fiber amplifiers (EDFAs), OXC, and OADM. Thus, each channel may experience unequal EDFA gains and different background shaping by the filters of OXC and OADM. The upshot is that the out-of-band ASE noise may not be equal to the in-band ASE noise (Fig.2.2). Besides, OSNR monitoring using a high-resolution OSA is costly, bulky, and inconvenient. To solve the last problem, several more compact out-of-band approaches based on arrayed-waveguide-grating (AWG) or tunable filters have been proposed.

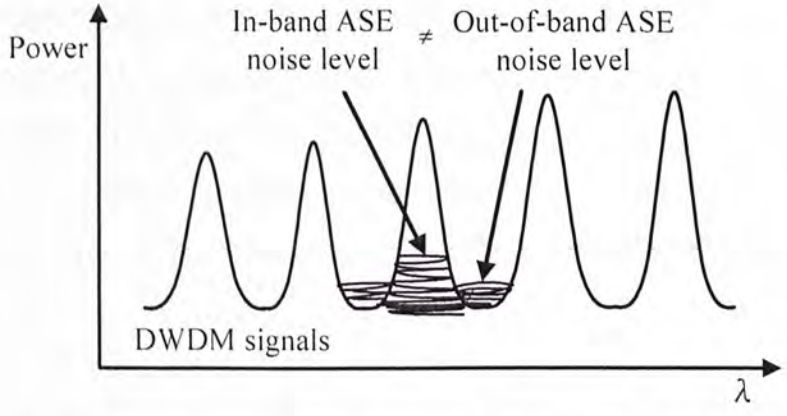

Figure 2.2: Out-of-band noise level may not be equal to in-band noise level in spectrum-interpolated noise measurement

2.2.2 Arrayed Waveguide Grating/Tunable Filter Assisted Power Measurements

An AWG module monolithically integrated with eight photodiodes was proposed in [32] to realize a compact OSNR monitor. The WDM signals are tapped and demultiplexed into individual signal wavelengths by the AWG. Each channel power is then detected and converted into a corresponding voltage by the photodiode. This voltage is proportional to the signal + ASE noise power of that channel. On the other hand, one of the ports of AWG is left unused and the voltage detected is proportional to the ASE noise power. With these two parameters, the OSNR can be calculated. However, the major problem of using AWG is the crosstalk issue when the channel number is large. To reduce the crosstalk, a double-resolution-AWG-based OSNR monitoring circuit was further proposed [33]. The OSNR could be monitored up to 37.5dB/0.1nm with <1-dB errors.

Another commonly used component in place of AWG is tunable filter [34]-[35]. The optical filtering approach usually uses two optical filters alternately: one with wide enough bandwidth to accommodate the signal spectrum for measuring the signal power and the other with narrow enough bandwidth to reject the adjacent channels for measuring the noise power. However, this requires filter with very deep transfer function for noise measurement. Recently, OSNR monitoring based on double-pass filtering and dithered tunable reflector has been proposed to solve this problem [36]. The OSNR can be monitored up to 44dB/0.1nm with errors <0.4 dB.

2.2.3 RF Spectral Analysis

2.2.3.1 Low/High RF Noise Monitoring

Another approach to out-of-band OSNR monitoring is to make use of the RF spectrum of the signal. This involves monitoring the signal power using an optical power meter and the electrical noise using an RF spectrum analyzer at spectral null locations at which the signal is not present. Both low-frequency (40-50 kHz) and high frequency (e.g. 9.8 GHz for 2.5 Gb/s signal) spectral null regions have been proposed in this regard [37]-[38]. OSNR monitoring using RF spectrum is simple and potentially low-cost. However, low-frequency monitoring suffers because it is susceptible to low-frequency noise tails that would exaggerate the strength of the noise. Moreover, it is suitable for signal with short pattern length only. On the other hand, high-frequency monitoring tends to suffer crosstalk from adjacent channels and may require high-speed RF spectrum analyzer as the data rates go up.

2.2.3.2 Subcarrier CNR Correlation

Alternatively, a subcarrier can be added out-of-band of the signal spectrum. The OSNR of the signal can be correlated to the electrical carrier-to-noise ratio (CNR) of the subcarrier [5]. This scheme is simple and allows simultaneous monitoring of multiple channels. However, the measurements are sensitive to dispersion effects such as CD and PMD due to high-frequency fading and the subcarrier consumes extra bandwidth.

2.3 In-band OSNR Monitoring Techniques

As we have discussed in Section 2.2.1, out-of-band OSNR monitoring is unreliable in dynamic reconfigurable networks and

tight-wavelength-spacing systems. Many approaches have thus been proposed to measure the in-band noise. All these methods rely on at least one of the following properties to differentiate the signal and noise: (i) signal is polarized while noise is unpolarized, (ii) signal is coherent while noise is incoherent, (iii) signal and noise have different duty cycles, and (iv) signal and noise are differently distributed in the phase space.

2.3.1 Polarization-Assisted OSNR Monitoring

Polarization-assisted OSNR monitoring is based on the principle that an optical signal has a well-defined polarization, whereas ASE noise is unpolarized as it is essentially white noise. Thus, polarization techniques can be employed to separate the signal and noise.

2.3.1.1 Polarization Extinction Method

In polarization extinction method [39], a polarization controller (PC) is used together with a polarizer in front of a tunable optical filter and a power meter (Fig. 2.3). The PC is adjusted until the power meter indicates minimum power, which corresponds to half the ASE power. Then the polarization controller is set to the orthogonal state and the power meter indicates the maximum power, which corresponds to the signal power plus half the ASE power. With the maximum and minimum power, OSNR can be calculated by

$$OSNR(\text{dB}/0.1\,\text{nm}) = \frac{P_{\max} - P_{\min}}{2P_{\min}} \tag{2.1}$$

where the NEB of the filter is assumed to be 0.1 nm. This method is simple and has no high-speed electronics processing, but it is susceptible to PMD degradation.

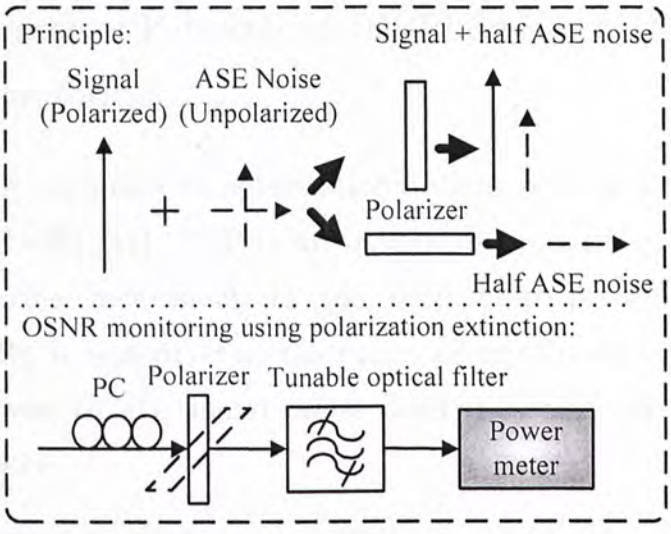

Figure 2.3: Principle and OSNR monitoring module using polarization extinction

2.3.1.2 Polarization-Nulling

Polarization-nulling is based upon the same principle as the polarization extinction method except that a rotating quarter-wave plate and a rotating linear polarizer are used to continuously searching for the maximum power and minimum power [40]. This method is simple, has large dynamic range, requires relatively low monitoring power, and has on-the-fly processing. However, it is also susceptible to PMD degradation.

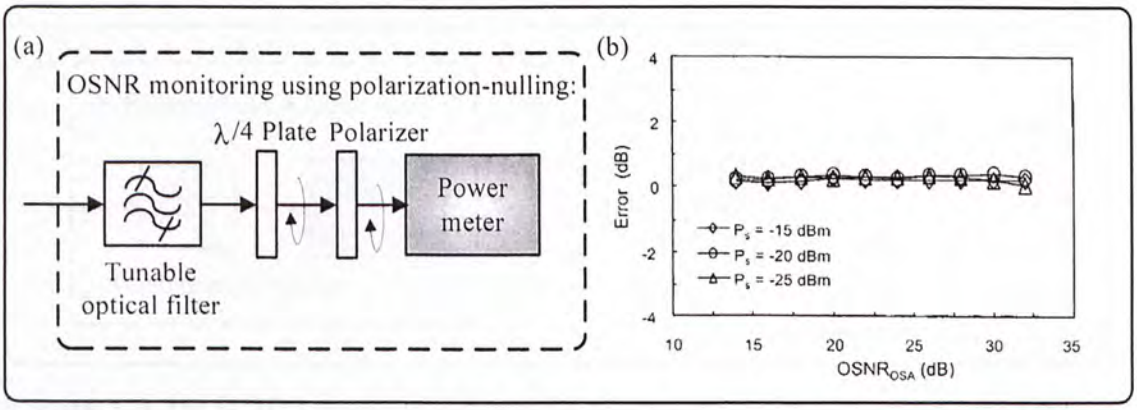

Figure 2.4: (a) OSNR monitoring module using polarization nulling (b) Monitoring results in a back-to-back configuration for six NRZ channels with errors < 0.4dB (Adapted from [40])

2.3.1.3 Degree-of-Polarization (DOP) Based OSNR Monitoring

Another slight variation to polarization-nulling is to use the degree-of-polarization (DOP) [41]. DOP is an important property of light sources used to describe how much of the total light power is polarized. Mathematically, it is defined as the polarized light power divided by the total light power, i.e. the signal power divided by the sum of signal and ASE noise power.

$$DOP = \frac{P_{\text{polarized}}}{P_{\text{total}}} = \frac{P_{\text{polarized}}}{P_{\text{polarized}} + P_{\text{unpolarized}}} = \frac{P_{\text{sig}}}{P_{\text{sig}} + P_{\text{ase}}} \tag{2.2}$$

Thus the in-band OSNR can be estimated from the DOP of a channel as follows:

$$OSNR = 10\log(\frac{DOP}{1 - DOP}) \tag{2.3}$$

The advantage of using DOP for in-band OSNR monitoring is that the information obtained can be used to monitor PMD as well. However, the monitoring dynamic range is small and DOP is significantly affected by PMD as well.

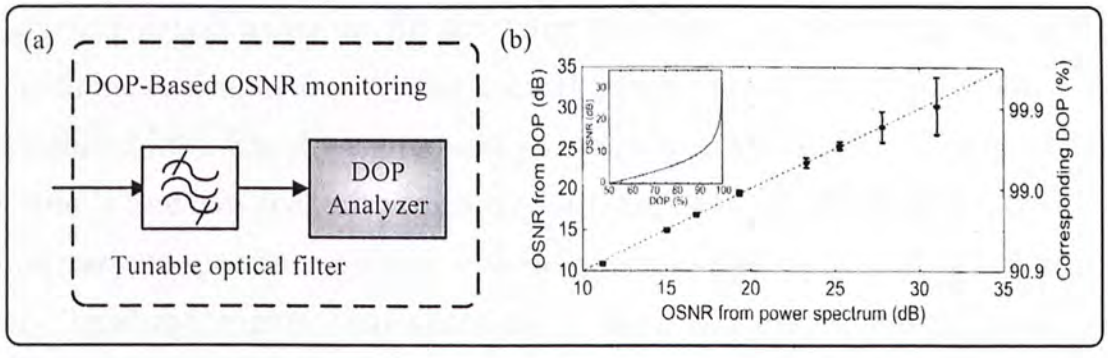

Figure 2.5: (a) DOP-based OSNR monitoring module (b) Monitoring errors in a back-to-back configuration with errors <1 dB up to 25dB/0.1nm (Adapted from Ref[41])

2.3.2 In-band RF Spectral Analysis

Another approach for in-band OSNR monitoring is to use in-band RF spectral analysis. There are two methods proposed: orthogonal delayed-homodyne method and half clock frequency constellation monitoring.

2.3.2.1 Orthogonal Delayed Homodyne Method

In orthogonal delayed homodyne method [42], a PMD emulator is added at the monitoring module and the PMD introduced will cause any given optical frequency component to split between the two orthogonal modes called principle states of polarization (PSP) and propagate down the fiber at different speeds. This speed differential, called the differential group delay (DGD), will dephase the given frequency component on each PSP with respect to the carrier and generate a dip in the electrical spectrum after detection due to destructive interference (Fig. 2.6). When the signal is launched at 45° (in Jones Space) relative to the PSPs, the minimum dip frequency is related to the DGD introduced by the PMD emulator by f_{min} = 1/(2**DGD*). By measuring this narrowband RF dip power (i.e. the electrical noise) using an RF spectrum analyzer, together with the total optical power measured by an optical power meter, the OSNR can be calculated [37]. Fig. 2.7 reproduces the experimental results. This method is simple and can deal with consider values of PMD. However, it requires a high rate of spectral analysis, obtains spectral nulling of the signal in a very localized region that contains a small amount of energy, and is sensitive to chromatic dispersion.

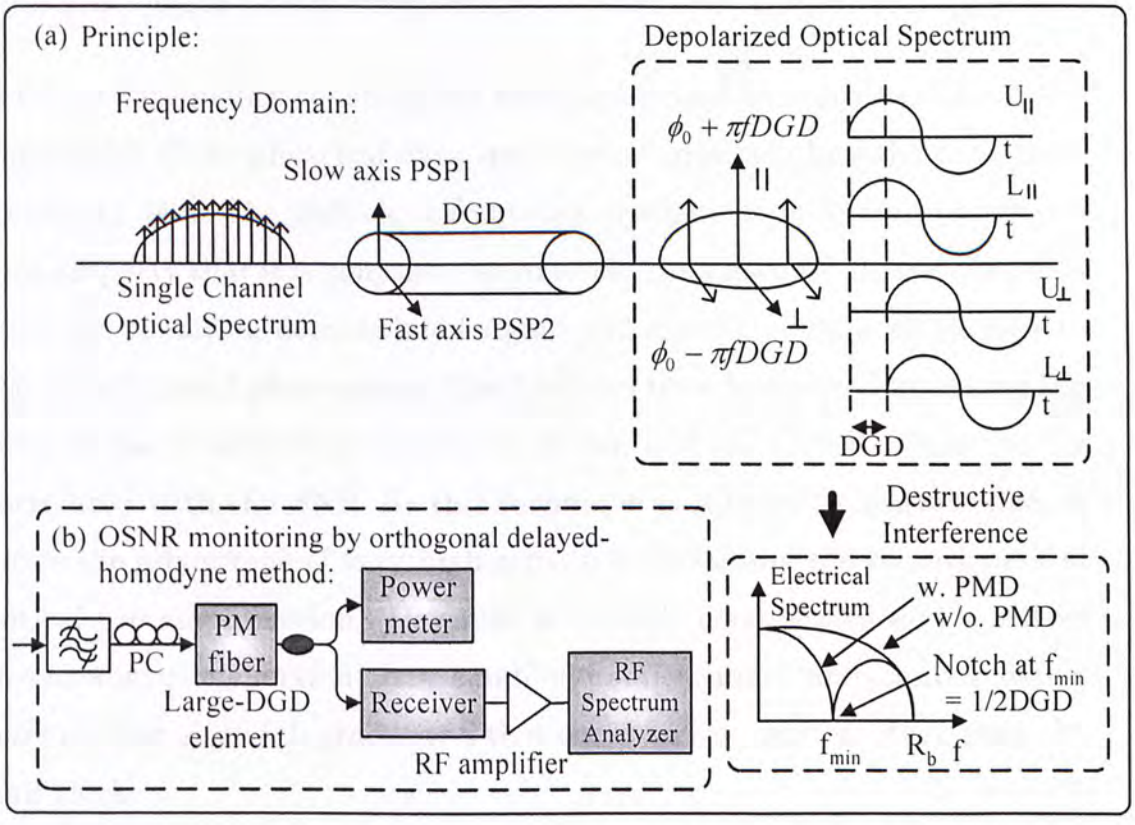

Figure 2.6: (a) Graphical representation of the generation of an RF spectral dip due to destructive interference when there is PMD (b) OSNR monitoring module by orthogonal delayed-homodyne method

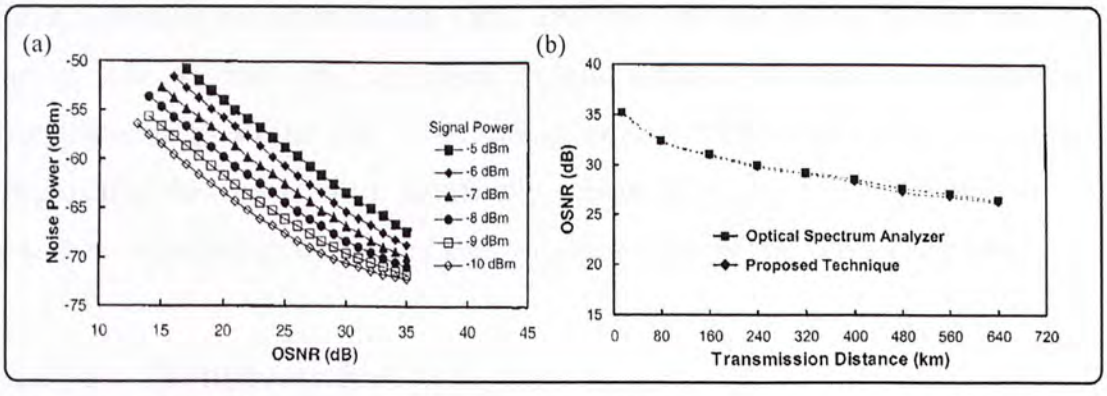

Figure 2.7: (a) Experimentally measured RF dip power versus OSNR (b) Measured OSNR versus transmission distance, errors <0.5 dB (Adapted from [42])

2.3.2.2 Half Clock Frequency Constellation Monitoring

Half clock frequency constellation monitoring uses an analysis of a narrow bandwidth of the electrical data spectrum at precisely half the data clock frequency [43]. The half clock frequency component is found to have the nice property that it is conjugate symmetric, thus if an RF demodulation is done the resulting demodulated signal will appear along a single axis in the demodulated phase-space. The SNR can then be derived by taking the ratio of the length of the line to its width, and the OSNR can be finally correlated with the SNR. As this technique is inherently narrowband, it offers the advantage of very high sensitivity (avoiding the requirement of optical pre-amplification). However, it is fairly complicated and sensitive to chromatic dispersion, has small dynamic range, and cannot detect narrowband signal degradations that occur at frequencies other than the half-clock.

2.3.3 Interferometric Approach

The third approach to differentiate the signal and noise is to use a Mach-Zehnder interferometer [44]. Due to the coherence of the optical signal, the signal can interfere at the output of the Mach-Zehnder interferometer while the ASE noise cannot. This method is simple, potentially low-cost, and relatively insensitive to PMD. However, it requires accurate matching of the coupling ratio of the 3-dB couplers.

2.3.4 Nonlinear Method

Nonlinear detection based on two-photon measurement can be used to monitor OSNR as well [45]. It is based on the concept that a PRBS signal has an average duty cycle less than 0.5 while the ASE noise has a duty

cycle of 1. As the average nonlinear signal produced is inversely proportional to the duty cycle, different OSNR will correspond to different average output power. This nonlinear detection method has high sensitivity, small polarization dependence, and bit-rate scalability. However, it has a small dynamic range and is affected by chromatic dispersion.

2.4 Polarization-Mode-Dispersion (PMD) Monitoring

PMD is another important optical parameter to be monitored in future optical networks. To a first-order approximation, PMD splits the optical pulses into two pulses polarized along the orthogonal PSPs and the two pulses will travel down the fiber at slightly different speeds. The resulting time difference is called the DGD [46]. The three major causes of PMD are (i) intrinsic geometric asymmetries in the fiber core, (ii) external mechanical stress-induced variations in the fiber core, and (iii) birefringence of in-line components. The intrinsic geometric asymmetries arise when slightly elliptical instead of perfectly circular optical fibers are manufactured. These asymmetries will remain fairly constant over time. On the other hand, the external mechanical stress-induced asymmetries stem from a variety of sources including daily and seasonal heating and cooling, nearby vibration sources, and periodic repair and maintenance. These asymmetries are typically dynamic in nature (Fig. 2.8).

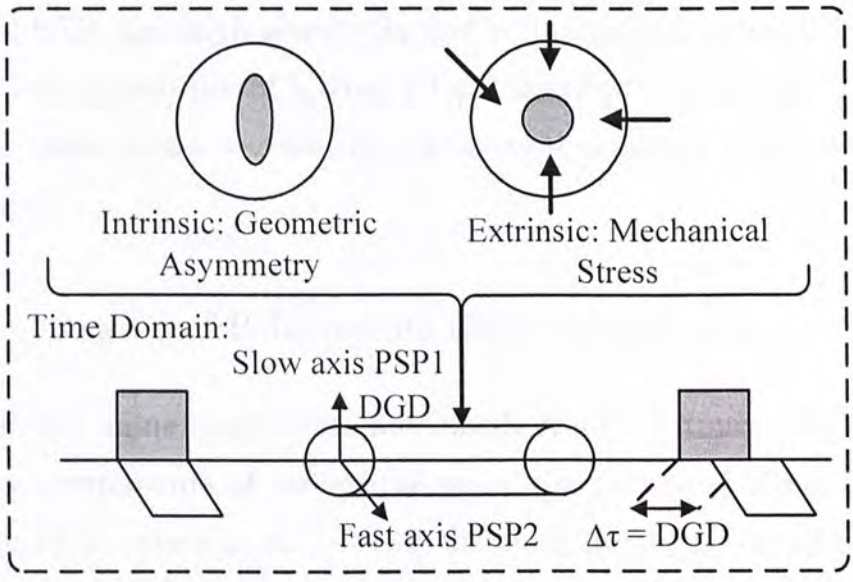

Figure 2.8: Graphic representation of the DGD between the two PSPs caused by intrinsic geometric asymmetry and extrinsic mechanical stress-induced asymmetry of the fiber core

PMD is a deleterious effect in high-speed (>10-Gb/s) optical systems because the splitting pulse will cause crosstalk and inter-symbol interference (ISI). It has been shown in several reports that the acceptable average DGD varies between 10% and 20% of a bit time depending mostly on the modulation format, outage probability, and receiver architecture [47]-[49]. It is particularly difficult to tackle PMD because the PMD effects are stochastic, time-varying, and temperature dependent, and worsen as the bit rate goes up. Moreover, instantaneous first-order PMD will follow a Maxwellian probability distribution which always has some finite possibility of severe system penalties. Although much of the fiber sold today is rated as "low PMD" fiber (< 0.1ps/√km), the presence of high-PMD legacy fiber and the PMD of in-line optical components make it necessary to monitor and compensate the effects of PMD.

Overall, desirable PMD monitoring methods should be simple, inexpensive, has fast monitoring speed (< ms), be highly correlated with

PMD and BER, has high sensitivity and wide dynamic range (~ bit time), and has low probability of hitting a local maximum [46],[50]-[51]. In the following subsections, we will review several reported PMD monitoring techniques.

2.4.1 Degree-of-Polarization (DOP) Monitoring

The DOP of a signal represents how much of all the time components or frequency components of an optical signal are polarized along the same SOP. The DOP varies from 1, when the components are polarized along the same SOP, to 0, when the polarizations of the components are randomly scrambled. The principle of using DOP for PMD monitoring is as follows: When a pulse having a DOP of 1 (polarized along the same SOP) enters at a 45° angle with respect to PSPs of a fiber with first-order PMD, the leading edge of the pulse is polarized along the fastest PSP, while the middle of the pulse has the same SOP as the input pulse, and the trailing edge is polarized along the slowest PSP. Hence the output optical signal is no longer polarized along the same SOP and DOP is degraded [52]. This is illustrated in Fig. 2.9 and Fig. 2.10.

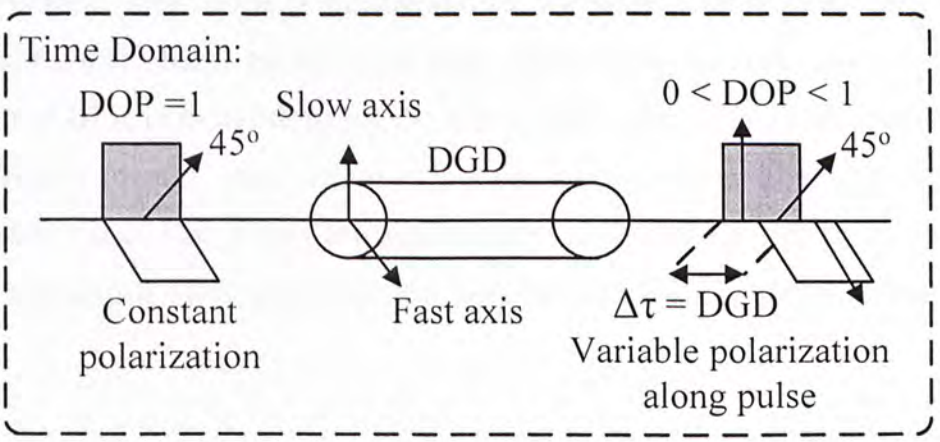

Figure 2.9: Impact of PMD on polarized optical signal and on its DOP

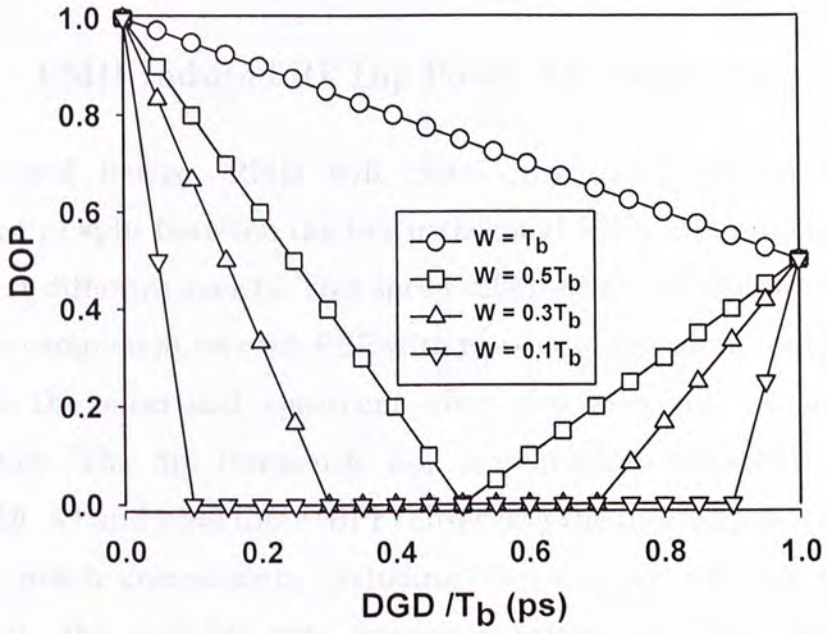

Figure 2.10: Theoretical results of minimum DOP versus DGD (relative to the bit time, T_b) as the pulse width (W) of an RZ signal varies, assuming ideal rectangular pulse

PMD monitoring based on DOP has a number of advantages including (i) it can be high-speed (kHz response time) and there is no need for high-speed electronics device, (ii) it is simple, (iii) it is bit-rate independent, and (iv) it is unaffected by chromatic dispersion and sign of the modulator chirp. However, it also suffers from several disadvantages including (i) it is dependent on the input SOP, and (ii) it is affected by the modulation format, magnitude of the modulator chirp, fiber nonlinearity, and ASE noise, (iii) it has low sensitivity for monitoring NRZ signal, and (iv) it has small dynamic range for monitoring RZ signal [46][50][66].

2.4.2 RF Spectral Analysis

2.4.2.1 PMD-Induced RF Dip Power Measurement

As explained before, PMD will cause any given optical frequency component to split between the two orthogonal PSPs and propagate down the fiber at different speeds. This speed differential will dephase the given frequency component on each PSP with respect to the carrier and generate a dip in the electrical spectrum after detection due to destructive interference. The dip frequency, f_{min}, is related to the DGD by $f_{min} = 1/(2*DGD)$. A band-pass filter (BPF) observing the intensity of a number of different notch components including the quarter bit rate frequency component, the half bit rate frequency component, and the bit rate frequency component can be used as first-order PMD monitors (Fig. 2.11) [53]-[59]. However, this method requires high-speed electrical circuits with the order of the bit rate and the sinusoidal PMD detection curve limits the maximum detection range. The method using multiple BPF is also proposed to widen the PMD detection range beyond 1-bit period but it has a more complicated compensation circuit and control algorithm [60].

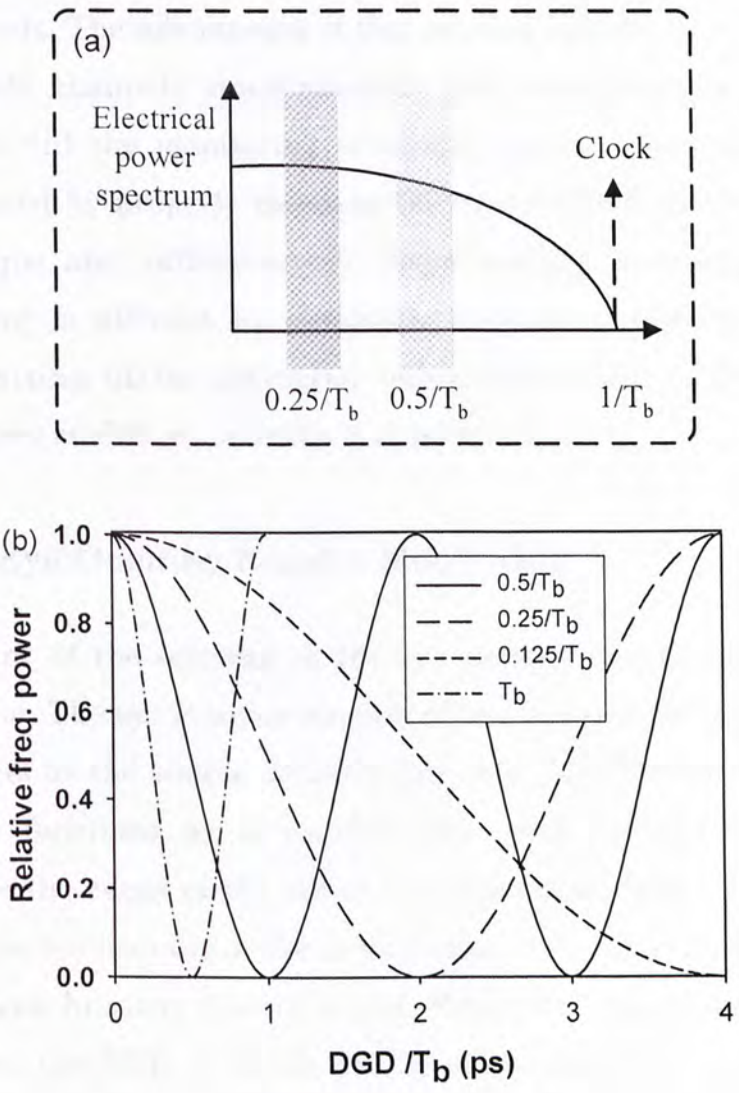

Figure 2.11: (a) Proposed different frequency components for PMD monitoring (b) Received RF power variation versus DGD for 1/8, quarter, half, and bit rate frequency components

2.4.2.2 Subcarrier-Based RF Power Fading Measurement

Subcarrier-based PMD monitoring allows simultaneous and independent PMD monitoring for WDM systems [61]. A subcarrier with the same power but slightly different frequency is added to each of the WDM channels. The subcarrier power fading due to PMD is strongly correlated to the PMD-induced degradation of that channel but is independent of that of

other channels. The advantages of this scheme include (i) it can monitor several WDM channels simultaneously and independently by a single module, and (ii) the monitoring sensitivity and dynamic range can be easily adjusted by properly choosing the subcarrier frequency. However, this technique also suffers several disadvantages including (i) the RF power fading is affected by chromatic dispersion, nonlinearities, and four-wave mixing, (ii) the subcarrier adds power penalty to the signal, and (iii) it requires modification at the transmitter side.

2.4.3 Eye-Opening Penalty Monitoring

Measurement of the opening in the eye pattern can be another useful PMD monitor. The eye monitor consists of two decision circuits in parallel. The first acts as the simple decision gate in a conventional receiver, and the second functions as a monitor gate with variable threshold to characterize the edges of the eye at variable phase. Since this technique evaluates the eye opening at the sample time, it needs a valid clock signal, called the synchronous control signal. While the eye opening is tightly correlated to the BER, it is affected by other distortion sources such as chromatic dispersion and nonlinearities [46],[50],[62]-[63].

2.4.4 Phase Diversity Detection

Phase diversity detection is an asynchronous method which measures the phase difference of a given frequency component after PSP filtering and electrical detection by using a Gilbert cell mixer. The PMD is then inferred from the measured phase. This detection scheme is not affected by other distortion sources such as chromatic dispersion. However, it requires PSP tracking at the receiver, which is fairly complicated, and is also affected by higher-order PMD [46], [64].

2.4.5 Arrival Time Measurement of Polarization-Scrambled Light

This method measures the arrival time variations of polarization-scrambled light by integrating the voltage-controlled oscillator (VCO) input signal of the clock recovery phase-locked loop (PLL) in the receiver. It allows detection of PMD at or below the eye pattern visibility limit, has high monitoring sensitivity, and is usable in the presence of higher-order PMD. However, it requires polarization scrambling at the transmitter and has small dynamic range [65].

2.4.6 Nonlinear Method

OPM based on nonlinear detection using two-photon absorption can monitor PMD in addition to OSNR [45]. Pulse splitting due to PMD increases the duty cycle of a pulse and thus change the average nonlinear output power. Nonlinear PMD monitoring has high sensitivity at small DGD values and bit-rate scalability. However, it is SOP dependent, sensitive to chromatic dispersion, and requires relatively high monitoring power to track the PMD fluctuations.

2.5 Summary of different OSNR and PMD Monitoring Methods

Fig. 2.12 summarizes the pros and cons of different proposed OSNR and PMD monitoring schemes.

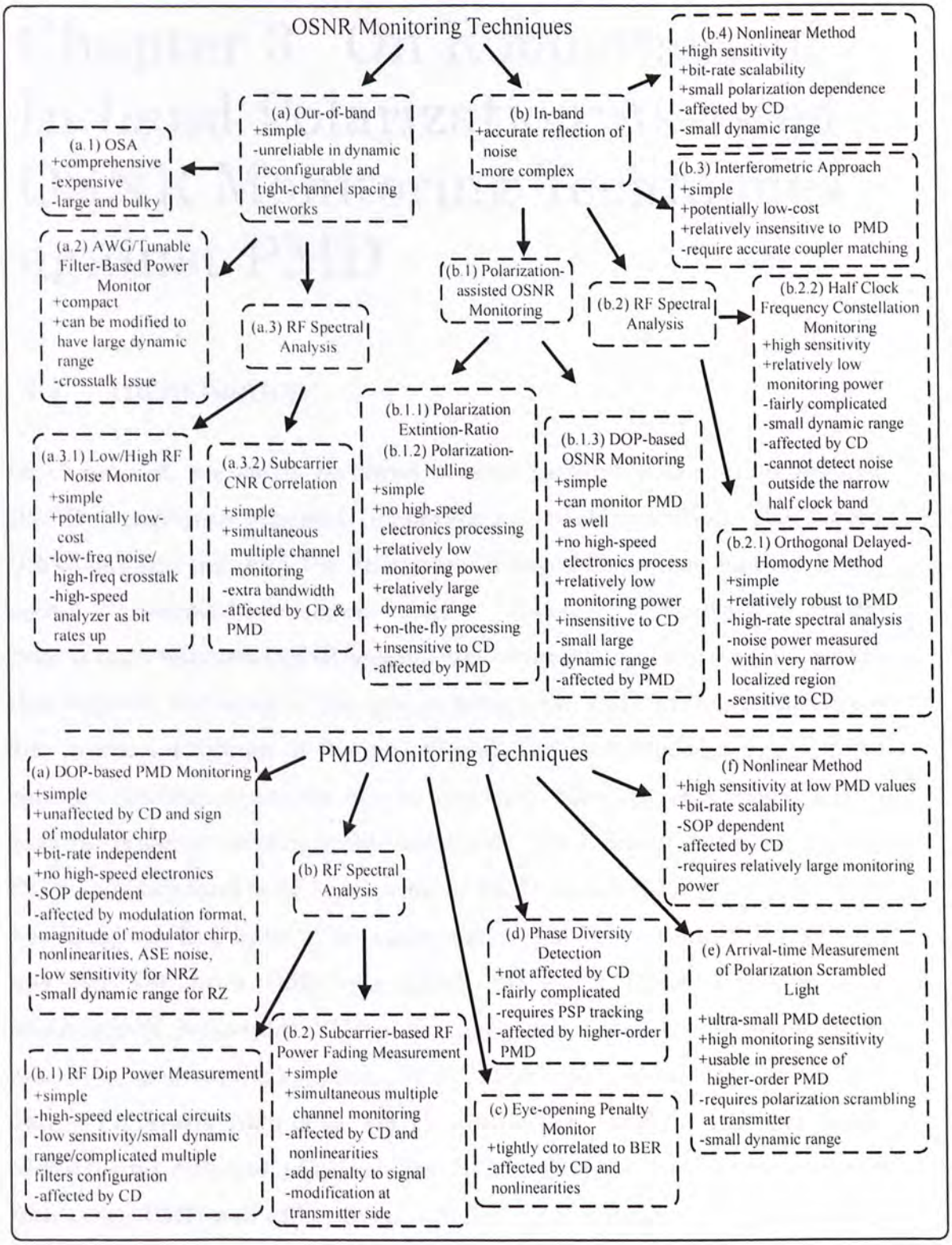

Figure 2.12: Summary of pros and cons of different OSNR and PMD monitoring schemes

Chapter 3 On Robustness of In-band Polarization-Assisted OSNR Monitoring Techniques against PMD

3.1 Introduction

In chapter 2, we have reviewed several in-band polarization-assisted OSNR monitoring schemes, including polarization-nulling, DOP-based OSNR monitoring, and the orthogonal delayed-homodyne method based upon polarization-assisted RF spectral analysis. These polarization-assisted OSNR monitoring techniques are meritorious in that they capture and analyze the true in-band noise and can thus avoid errors due to mis-estimation of the out-of-band ASE noise springing from tight channel spacing, crosstalk due to improper filtering, or unequal EDFA gain in dynamic reconfigurable networks. The tradeoff, however, is that these schemes tend to be susceptible to PMD degradation. This PMD issue has been touched upon in previous papers but the extent of degradation has not yet been fully quantified. Since all these schemes must demonstrate reasonable PMD robustness before they can be deployed in real high-speed optical systems, it would be highly desirable if we have a detailed quantification of the OSNR monitoring errors for different degree of PMD and different pulse widths. In this chapter, we will explain how first-order PMD will affect these schemes and evaluate, both numerically and experimentally, the robustness of the three aforementioned in-band OSNR monitoring schemes against PMD for 10-Gb/s NRZ, 30% RZ, and 3% RZ signals. Our experimental results show that polarization-nulling

and DOP-based OSNR monitoring are extremely sensitive to the influence of PMD – For 1-dB OSNR monitoring error (original OSNR: 25dB/0.1nm), the maximum tolerable DGD values for 10-Gb/s NRZ, 30% RZ, and 3% RZ signals are <10 ps, <3 ps, and <0.5 ps, respectively. On the other hand, orthogonal delayed homodyne method exhibits an inherent robustness hinting at the feasibility to drastically improve the performance of the former two schemes. The numerical calculations and experimental results are presented for the three methods in the following sections.

3.2 Impact of PMD on Polarization-Nulling

To a first-order approximation, PMD can be described as a DGD between the two orthogonal polarization modes of the fiber. The DGD of the fiber link will rotate the frequency components of the signal with respect to the carrier by an amount equal to $\pi * \Delta f * DGD$ (in Jones space), where Δf is the frequency offset from the center carrier, when the signals are launched at a 45° with respect to the PSPs [67]. This is referred to as the SOP walk-off effect. Consequently, in polarization-nulling when we align a polarizer parallel to the signal, the maximum power (signal + ½ ASE noise power) will be underestimated because the polarizer is aligned with a single SOP only. Similarly, when we align a polarizer perpendicular to the signal, the minimum power (½ ASE noise power) will be overestimated. This is illustrated in Fig. 3.1.

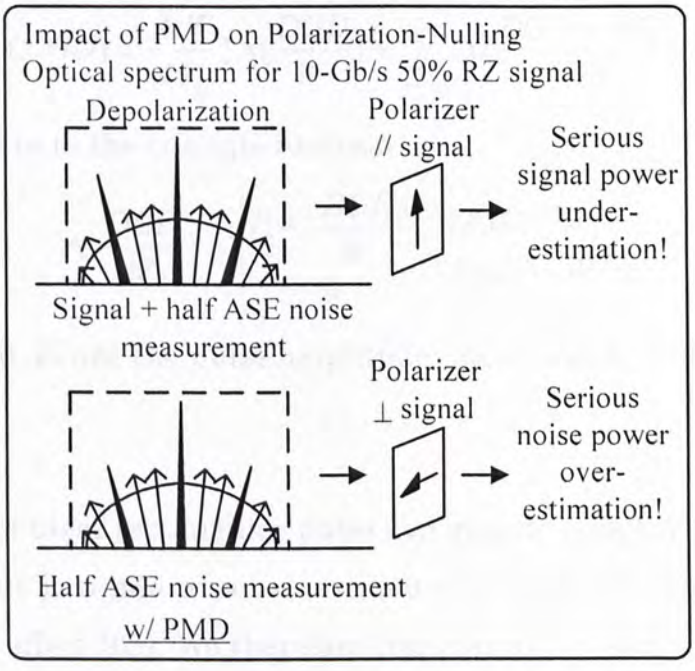

Figure 3.1: Impact of PMD on Polarization-Nulling

The polarization leakage ratio, α, which represents how much proportion of the signal power intrudes into the noise measurement, can be calculated by [6][39]

$$\alpha = \frac{\int_{-\infty}^{\infty} \sin^2(\pi * f * DGD) S(f) df}{\int_{-\infty}^{\infty} S(f) df} \tag{3.1}$$

where $S(f)$ is the optical power spectral density. By expressing the sine term in (3.1) as the sum of two exponential terms and taking the inverse Fourier transform, α can be related to the autocorrelation function of the received optical signal R_{in} as

$$\alpha = \frac{2R_{in}(0) - R_{in}(DGD) - R_{in}(-DGD)}{4R_{in}(0)} \tag{3.2}$$

The autocorrelation R_{in} is dependent on the pulse shape and pulse width. For ideal rectangular pulses, the general expression for the autocorrelation function for an RZ signal is given in [68]:

$$R_{in}(DGD) = \frac{A^2 W}{4T_b}[\Lambda(\frac{DGD}{W}) + \sum_{m=-\infty}^{\infty} \Lambda(\frac{DGD - mT_b}{W})] \qquad (3.3)$$

where Λ refers to the triangle function

$$\Lambda(\frac{DGD}{W}) = \begin{cases} (1 - \frac{|DGD|}{W} & |DGD| < W \\ 0 & |DGD| > W \end{cases} \qquad (3.4)$$

and A, W, and T_b are the pulse amplitude, pulse width, and bit duration, respectively.

The use of ideal rectangular pulse can greatly simplify the numerical calculation but it would also overestimate the power leakage due to the SOP walk-off effect [69]. We therefore consider also a second type of pulse shape, the super-Gaussian pulse shape, of which the normalized amplitude is expressed as [70]

$$U(T) = \exp\{-\frac{1+iC}{2}(\frac{T}{T_{FWHM}/1.763})^{2m}\} \qquad (3.5)$$

where U is the intensity of the super-Gaussian pulse, C is the chirp parameter, T_{FWHM} is full-width at half maximum of amplitude, and m is the Gaussian pulse order. The autocorrelation of super-Gaussian pulse shape is more complicated and we will implement the details using the Matlab6.1 software.

3.2.1 Numerical Results using Ideal Rectangular Pulse

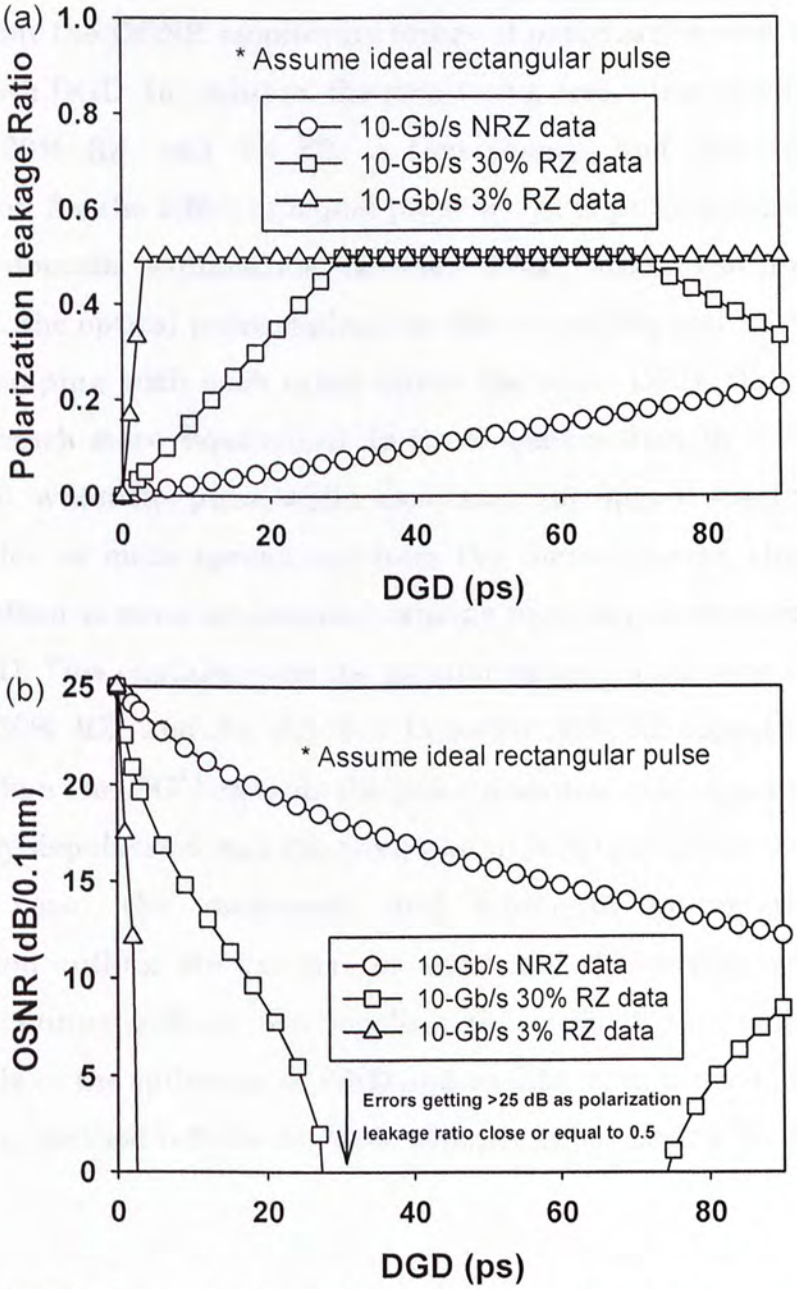

Figure 3.2: (a) Theoretically calculated polarization leakage ratio and (b) OSNR under different DGD values, assuming ideal rectangular pulse

Fig. 3.2(a) and Fig. 3.2(b) show the theoretically calculated polarization leakage ratio and OSNR (original OSNR: 25dB/0.1nm), respectively, under different DGD values using ideal rectangular pulse. From Fig. 3.2(b), we can see that the OSNR monitoring errors of polarization-nulling increase rapidly with DGD. In addition, the monitoring errors increase in the order of NRZ, 30% RZ, and 3% RZ. A time-domain and frequency-domain explanation for the effect of signal pulse width is provided in Fig. 3.3. In the time-domain explanation in Fig. 3.3(a), when the pulse width decreases, the optical pulse replicas on the two orthogonal PSPs will have less overlapping with each other under the same DGD, thus the signal becomes much more depolarized. In the frequency-domain explanation in Fig. 3.3(b), when the pulse width decreases, the optical spectrum will be much wider or more spread out from the center carrier, thus the SOP walk-off effect is more pronounced causing more depolarization under the same DGD. This explains why the monitoring errors increase in the order of NRZ, 30% RZ, and 3% RZ. For Consider 30% RZ signal and 3% RZ signal. When the DGD exceeds the pulse duration, the signal will become completely depolarized and the polarization leakage ratio is 0.5 (Fig. 3.2). In this case, the maximum and minimum power recorded in polarization-nulling are exactly the same and the corresponding OSNR would be minus infinity. We conclude that polarization-nulling is very susceptible to the influence of PMD and modification is needed before this monitoring method is to be deployed practically, especially for RZ systems.

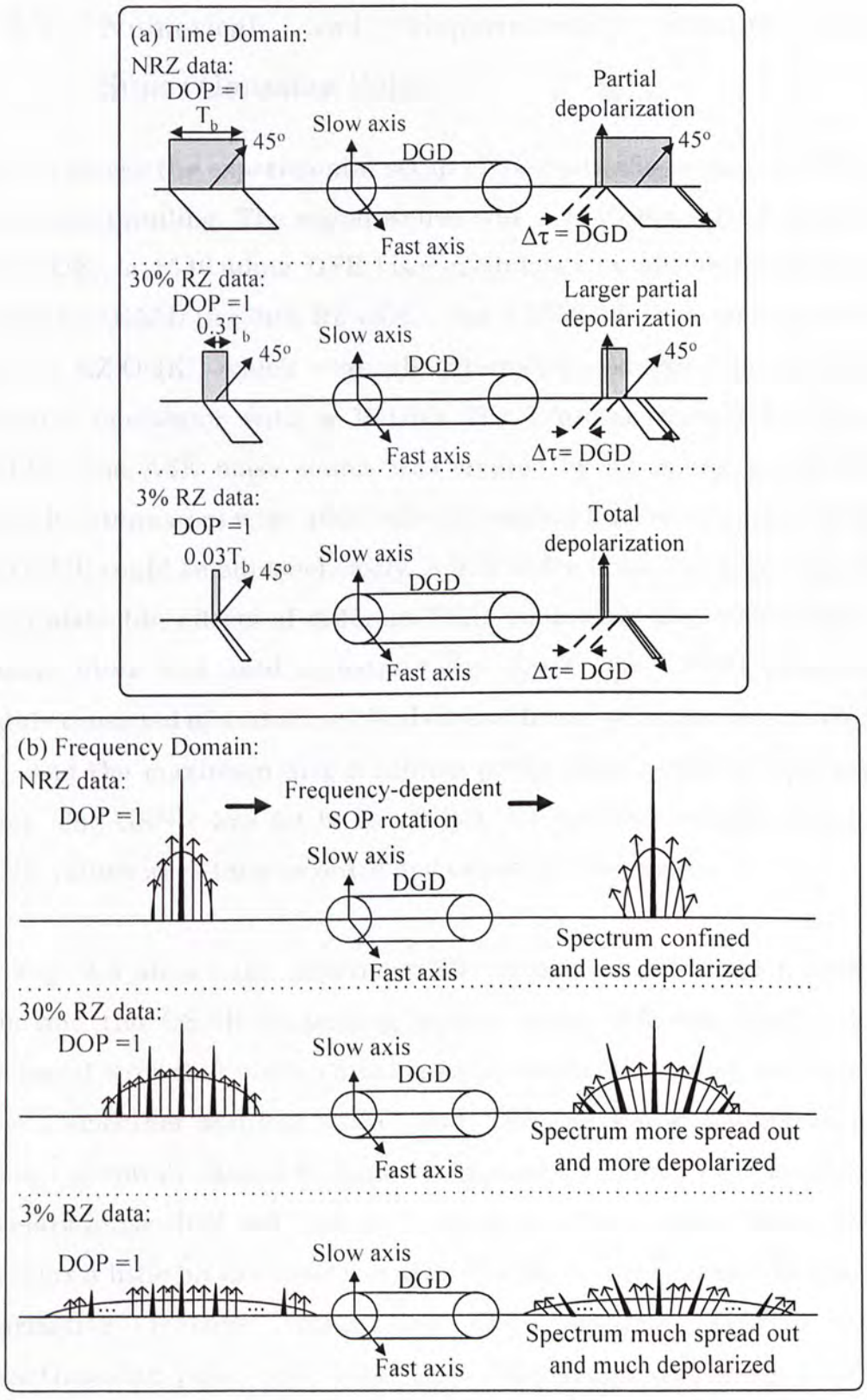

Figure 3.3: (a) Time-domain and (b) frequency-domain explanation of the depolarization effect for different pulse widths under the same DGD

3.2.2 Numerical and Experimental Results using Super-Gaussian Pulse

Fig. 3.4 shows the experimental setup to evaluate the impact of PMD on polarization-nulling. The signal source was a 1546.46nm DFB laser (for NRZ-OOK), a 1546.46nm DFB laser modulated by an electroabsorption modulator (EAM) (for 30% RZ-OOK), and a 1552.33nm mode-locked laser (for 3% RZ-OOK), which were all externally modulated by a $LiNbO_3$ intensity modulator with a 10-Gb/s 2^{31} -1 pseudorandom bit stream (PRBS). The ASE noise source was created by cascading two EDFAs. Variable attenuators were added after the signal and noise sources so that the OSNR could be adjusted easily. A first-order PMD emulator was used to simulate the effects of different DGD values. At the receiver side, a tunable filter was used to extract the signal. The OSNR monitoring module consisted of a rotating $\lambda/4$ plate and linear polarizer, as reported in [40], and the maximum and minimum power were recorded by a power meter. The OSNR was set to be 25dB/0.1nm by OSA and the measured OSNR values were then recorded and calculated for errors.

Fig. 3.5 shows the experimentally measured polarization leakage ratio and the OSNR monitoring results under different DGD values. Compared with that obtained using ideal rectangular pulse, both curves show a smoother and less steep trend. This is because the polarization leakage is mainly caused by higher frequency components at the edges of the mark pulses [66] and the use of less steep pulse in actual transmission can relax a little bit the depolarization. The theoretical calculations for the polarization leakage ratios and the converted OSNRs using super-Gaussian pulse with order 2 for NRZ signal and order 1 for RZ signal are also shown in Fig. 3.5 (straight lines). For NRZ pulse, the experimental results and theoretical calculations are in excellent

agreement. For 30% RZ pulse, when the DGD approaches half bit time, the experimental results and theoretical calculations show slight deviation because the experimentally used pulse is not purely super-guassian, but is super-guassian with a small "tail" in the time domain. This tail increases the overlapping of the two orthogonal optical pulses and hence relaxes a little bit the depolarization extent. For the 3% RZ pulse, the polarization leakage ratio is theoretically calculated to be 0.5 and the converted OSNR is negative infinity at large DGD values. However, in actual experiments, the maximum measured power and minimum measured power after the polarizer in polarization-nulling will always show some difference due to fluctuations of the power meter. Hence the maximum OSNR errors saturate at some finite values (Fig. 3.5(b)). For a 1-dB OSNR monitoring error, the maximum tolerable DGD values for NRZ, 30% RZ, and 3% RZ are found to be <10 ps, <3 ps, and <0.5 ps, respectively.

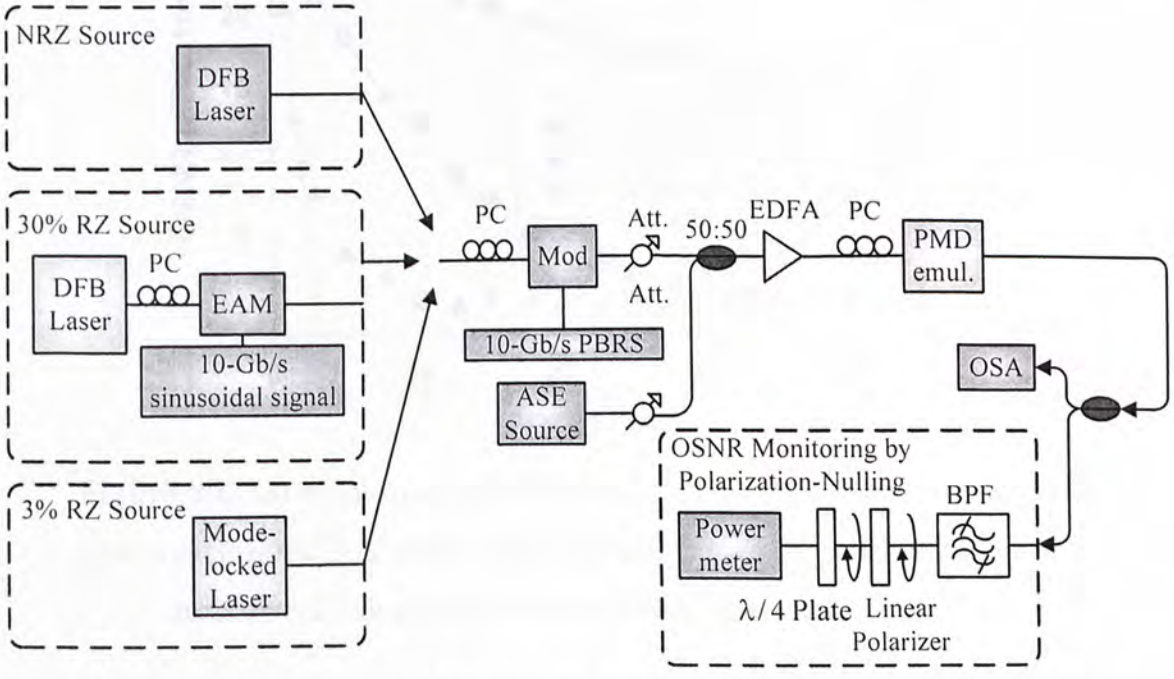

Figure 3.4: Experimental setup to evaluate OSNR monitoring based on polarization-nulling under different DGD values

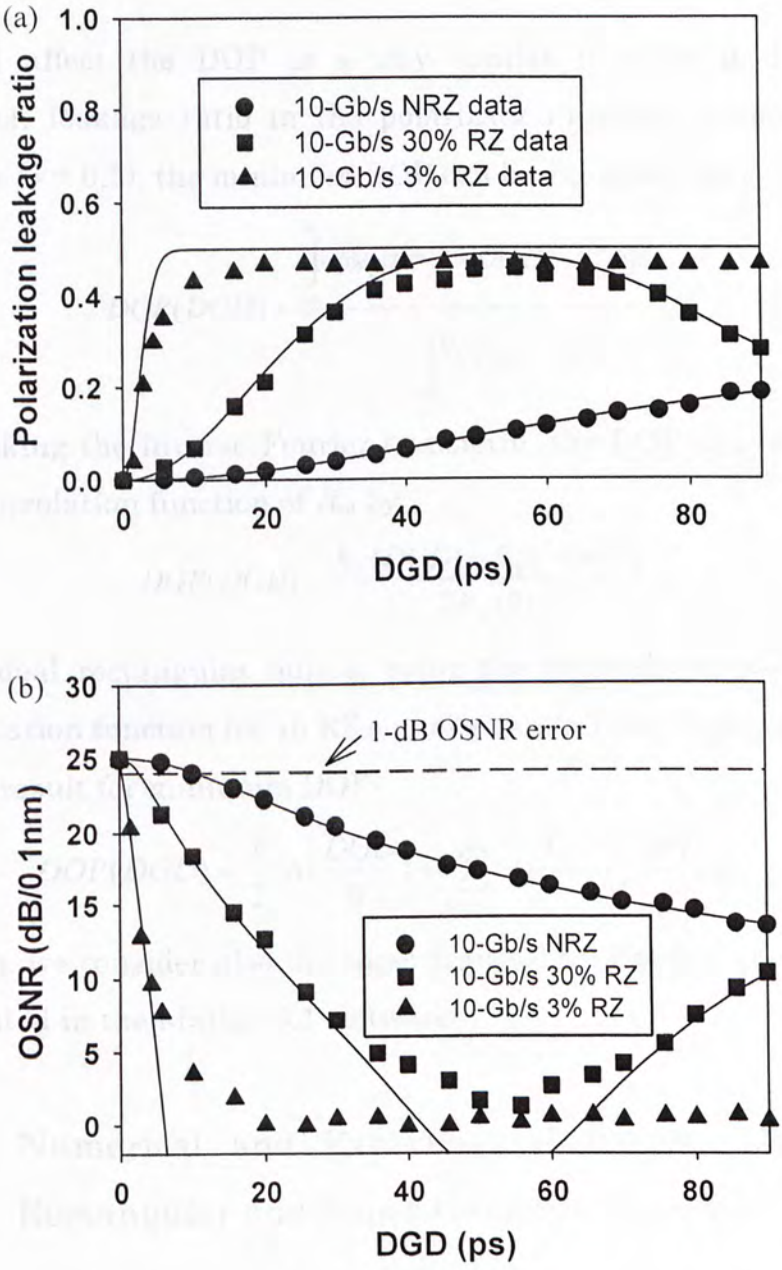

Figure 3.5: (a) Measured polarization leakage ratio and (b) OSNR for polarization-nulling under different DGD values (Straight lines: numerical calculations using Super-Gaussian pulse)

3.3 Impact of PMD on DOP-based OSNR Monitoring

PMD will affect the DOP in a way similar to what it does to the polarization leakage ratio in the polarization-nulling method. For the worse case ($\gamma = 0.5$), the minimum DOP can be expressed as:

$$DOP(DGD) = \frac{\int_{-\infty}^{\infty} \cos(2\pi * f * DGD) S(f) df}{\int_{-\infty}^{\infty} S(f) df} \tag{3.6}$$

By taking the inverse Fourier transform, the DOP can be related to the autocorrelation function of R_{in} by

$$DOP(DGD) = \frac{R_{in}(DGD) + R_{in}(-DGD)}{2R_{in}(0)} \tag{3.7}$$

For ideal rectangular pulses, using the general expression for the autocorrelation function for an RZ signal given in Eqn. (3.3), we obtain the following result for minimum DOP:

$$DOP(DGD) = \frac{1}{2}[\Lambda(\frac{DGD}{W}) + \sum_{m=-\infty}^{\infty} \Lambda(\frac{DGD - mT_b}{W})] \tag{3.8}$$

Again, we consider also the super-Gaussian pulse and the details are implemented in the Matlab 6.1 software.

3.3.1 Numerical and Experimental Results Using Ideal Rectangular and Super-Gaussian Pulses

The experimental setup used to evaluate the effect of PMD on DOP-based OSNR monitoring was similar to that described in previous section except the monitoring module now consisted of a tunable filter and a DOP analyzer. The theoretical calculated DOP degradation and the corresponding OSNR under different DGD values using ideal rectangular pulse and super-Gaussian pulse were shown in Fig. 3.6 and Fig. 3.7,

respectively. Experimental results were also presented in Fig. 3.7.

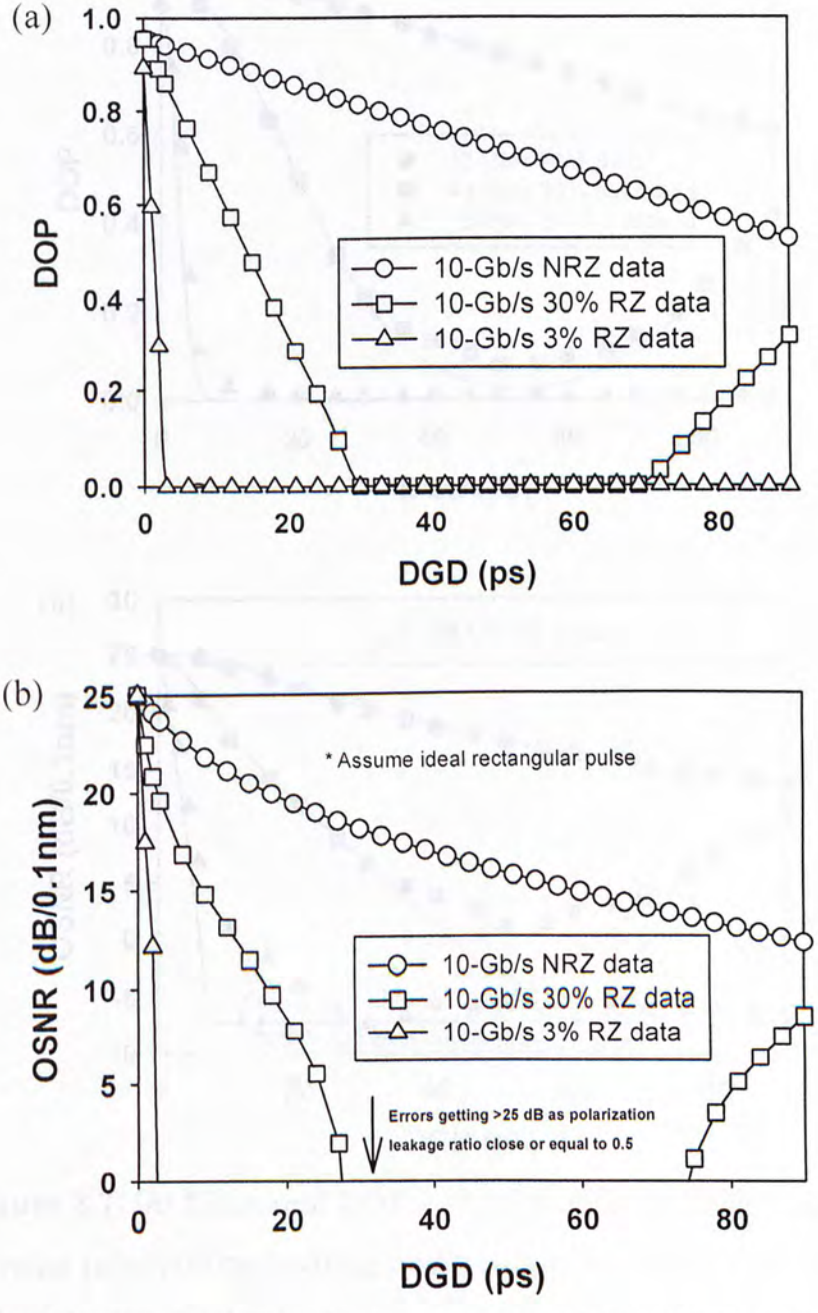

Figure 3.6: (a) Theoretically calculated DOP and (b) OSNR under different DGD values, assuming ideal rectangular pulse

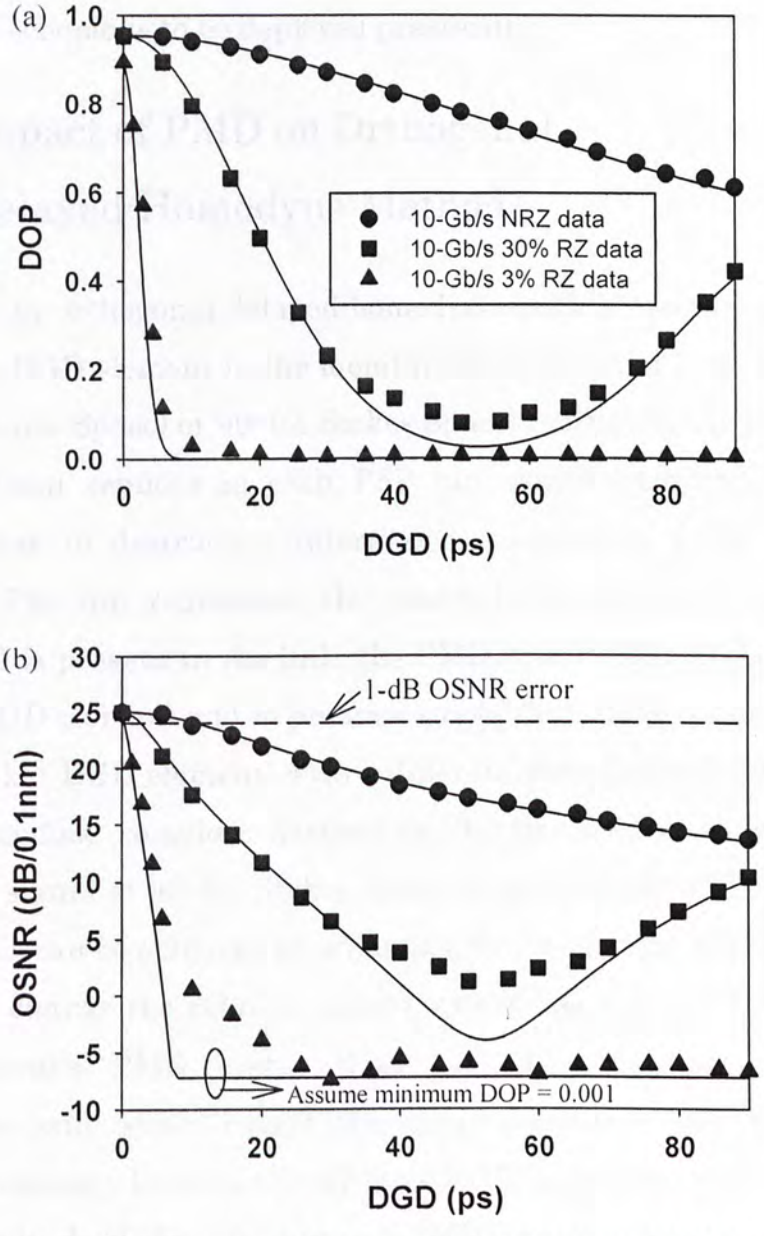

Figure 3.7: (a) Measured DOP and (b) OSNR for DOP-based OSNR monitoring polarization-nulling under different DGD values (Straight lines: numerical calculations using Super-Gaussian pulse)

It is found that the monitoring errors for DOP-based OSNR monitoring are similar to that in polarization-nulling because they are based upon the same principle. Thus DOP-based OSNR monitoring is also

susceptible to PMD degradation and modification is needed before the monitoring scheme is to be deployed practically.

3.4 Impact of PMD on Orthogonal Delayed-Homodyne Method

Recall that in orthogonal delayed-homodyne method (section 2.3.2.1), we use a large-DGD element in the monitoring module and launch the signal at 45° (in Jones Space) or 90° (in Stokes Space) relative to the PSPs so that the two signal replicas in each PSP can cancel each other after RF detection due to destructive interference to produce a dip in the RF spectrum. The dip represents the narrowband electrical noise power. When PMD is present in the link, the PMD vector of the link and that of the local DGD element add to produce a resultant PMD vector of the total system (link + DGD element) with a different direction and amplitude. In order to produce complete destructive interference, it is necessary to launch the signal at 90° (in Stokes Space) relative to the PSPs of the total system. This can be achieved by adjusting the PC in front of the local DGD element to change the relative angle between the link's PMD vector and DGD element's PMD vector (Fig. 3.8). In this case, destructive interference still occurs except the minimum dip is now located at a different frequency because the effective DGD is changed and is now equal to the magnitude of the total system's PMD vector.

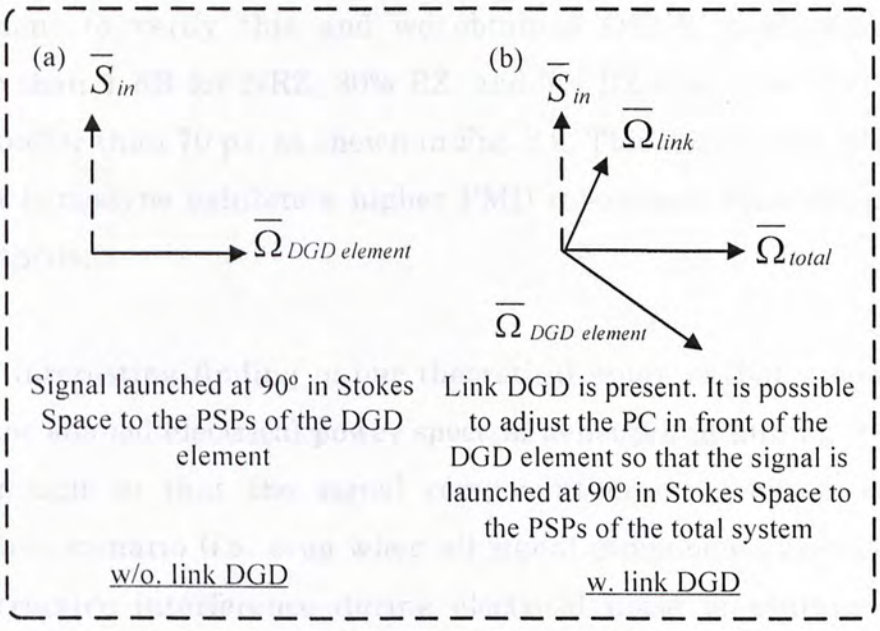

Figure 3.8: PMD vectors (a) when there is no link DGD (b) when there is link DGD.

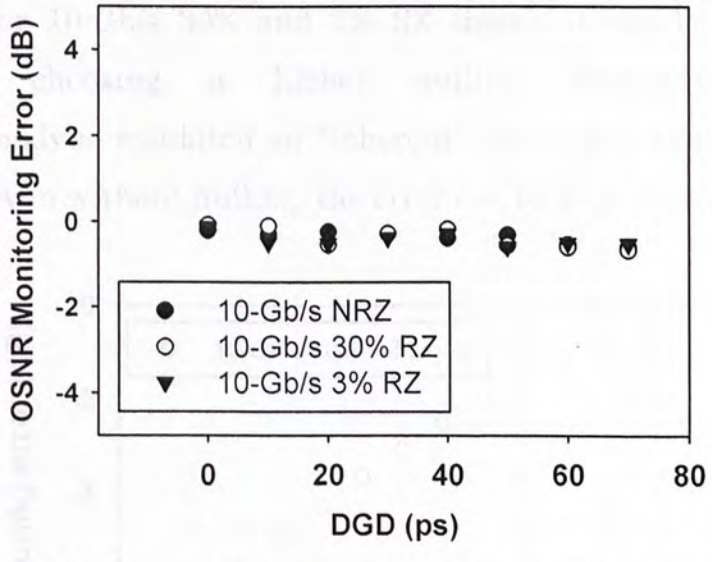

Figure 3.9: OSNR monitoring error for orthogonal delayed-homodyne method under different DGD

Thus, PMD will change the dip frequency and is expected to cause insignificant errors for this method so long as destructive interference can still occur and the minimum dip power obtained. We performed

experiment to verify this and we obtained OSNR monitoring errors smaller than 1 dB for NRZ, 30% RZ, and 3% RZ when the DGD values were smaller than 70 ps, as shown in Fig. 3.9. This shows that orthogonal delayed homodyne exhibits a higher PMD robustness than the previous two methods.

An interesting finding in our theoretical study is that assuming an ideal sinc-shaped electrical power spectral density and nulling frequency high enough so that the signal component becomes small, even for worst-case scenario (i.e. even when all signal components are not nulled by destructive interference during electrical noise measurement), the monitoring errors can be kept below certain dB which is much smaller than that in polarization-nulling method. For example, Fig. 3.10 shows the theoretically calculated largest monitoring errors against nulling frequency for 10-Gb/s 30% and 3% RZ signal. It can be seen that by judiciously choosing a higher nulling frequency, orthogonal delayed-homodyne exhibited an "inherent" robustness against PMD in a sense that even without nulling, the error can be kept reasonably small.

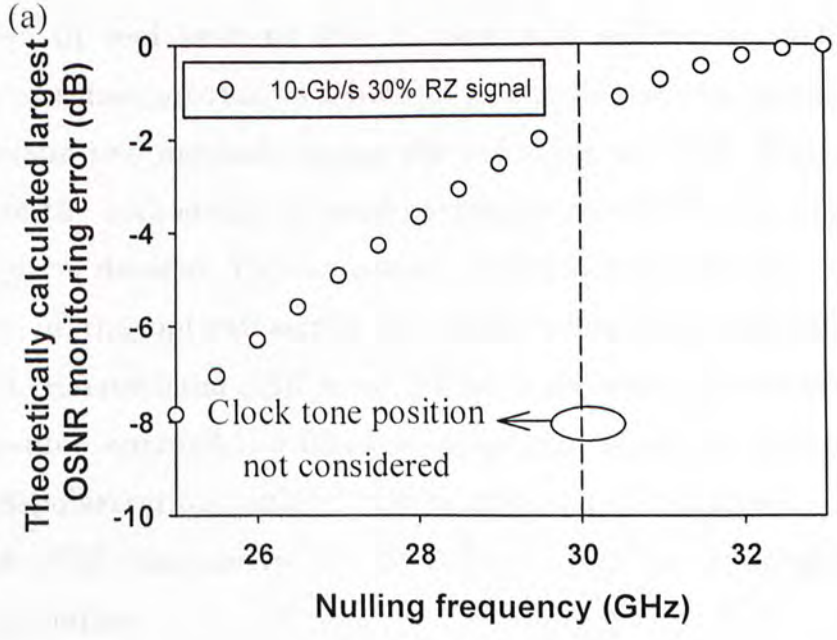

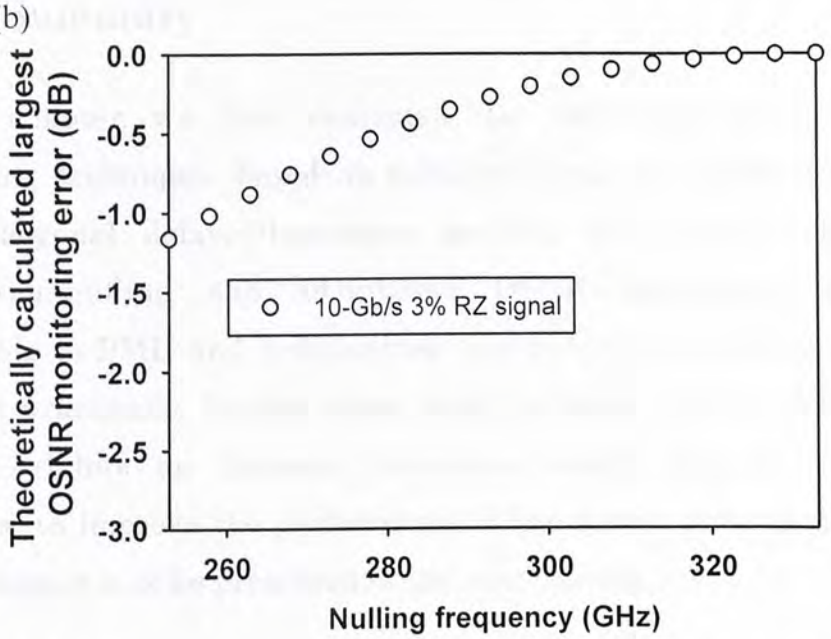

Figure 3.10: Theoretical calculated worst OSNR error against nulling frequency for orthogonal delayed homodyne method for (a) 10-Gb/s 30% RZ signal and (b) 10-Gb/s 3% RZ signal, assuming ideal rectangular pulse and ideal sinc-shaped RF spectrum

Although this inherent PMD robustness is based on the assumption of ideal rectangular pulse and hence ideal RF spectrum and may not be attainable in real systems due to expensive nulling at such high RF frequency, it does provide us a hint on how to improve the performance of the previous two methods under the influence of PMD. This method is similar to the orthogonal delayed-homodyne method but is implemented in the optical domain. We can use an optical narrowband filter placed at the edge of the optical signal spectrum before polarization-nulling to obtain the narrowband ASE noise. Because the signal power extracted by the off-center narrowband filter is inherently small, the signal leakage due to depolarization under PMD is expected to be small. This newly proposed PMD-insensitive OSNR scheme will be elucidated in the following chapter.

3.5 Summary

In this chapter, we have evaluated the PMD robustness of OSNR monitoring techniques based on polarization-nulling, DOP correlation, and orthogonal delayed-homodyne method. Our studies show that polarization-nulling and DOP-based OSNR monitoring are very susceptible to PMD and modifications are needed before they are to be deployed practically. On the other hand, orthogonal delayed-homodyne method exhibits an inherent robustness which inspires us a new technique to improve the performance of the former two schemes. This new technique is to be presented in the next chapter.

Chapter 4 PMD-Insensitive OSNR Monitoring Based on Polarization-Nulling with Off-Center Narrowband Filtering

4.1 Introduction

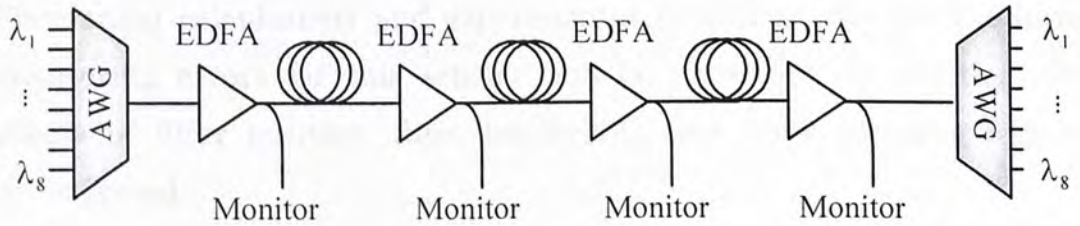

Figure 4.1: Schematic diagram of a typical transmission link

Fig 4.1 shows the schematic diagram of a typical transmission link in real systems. As shown in Fig. 4.1, OSNR monitoring is performed after each amplifier site. However, since PMD compensation may not be available after each amplifier site, the effect of PMD should not be neglected. Nevertheless, we found in chapter 3 that several of the in-band polarization-assisted OSNR monitoring schemes, including polarization-nulling and DOP-based OSNR monitoring, were significantly impinged on by the depolarization effect of PMD. This PMD depolarization will reduce, respectively, the maximum-minimum power ratio and the DOP in the two aforementioned methods and hence cause the OSNR to be underestimated. A serious underestimation of OSNR may trigger

unnecessary signal-degradation alarms and rerouting mechanisms, and creating potential legal contract violation and financial burden for service providers. Much research endeavor has therefore been made to decouple OSNR and PMD in order to enable accurate, PMD-insensitive in-band OSNR monitoring. In this chapter, we will first review two previously proposed schemes, namely, improved polarization-nulling and periodic polarization encoding. Although PMD insensitivity was reported, these two schemes both require a complex configuration. We will then describe our newly proposed PMD-insensitive OSNR monitoring scheme based on polarization-nulling with off enter narrowband filtering. Compared with previous schemes, our scheme employs a simpler configuration and is more readily upgradeable for use in higher data-rate optical systems. Theoretical calculations and experimental results on the PMD-induced monitoring errors for this scheme will be presented. In addition, the effects of filter position, filter bandwidth, and filter detuning will be investigated.

4.2 Previously Proposed Schemes based on Polarization-Nulling

4.2.1 Improved Polarization-Nulling Technique

The first proposed method, improved polarization-nulling [71], makes use of three receivers and an additional BPF to separate the two contributions – ASE noise and PMD-induced signal power leakage, when measuring the minimum power. The proposed technique is shown in Fig. 4.2(a). The demultiplexed WDM signal was sent to the PBS via an automatic PC. The PC was used to maximize the signal power in one arm of the PBS. Thus, the signal and ASE noise were split into two polarization components (in which one polarization consists of signal and

ASE noise, while the other has ASE noise only). The ASE noise-only branch is further split into two arms with one arm additionally filtered by a BPF to change the optical bandwidth. Assuming the signal leakage in the latter two branches is the same, any change in the measured power should be due to ASE noise difference; the contribution by the signal power leakage can therefore be eliminated. Mathematically, the output powers of the three branches are

$$P_1 = P_s(1-\varepsilon) + 0.5P_{ase} \tag{4.1}$$

$$P_2 = 0.5P_s\varepsilon + 0.25P_{ase} \tag{4.2}$$

$$P_3 = 0.5P_s\varepsilon + 0.25\alpha P_{ase} \tag{4.3}$$

where P_s and P_{ase} are the signal power and ASE noise power in watts, respectively. ε is the signal leakage ratio. α is determined by the transmission characteristics of AWG and BPF. Using equations (4.1)-(4.3), the OSNR can be obtained as:

$$OSNR = \frac{P_s}{P_{ase}} = \frac{(P_1 + 2P_2)}{4(P_2 - P_3)/(1-\alpha)} - 1 \tag{4.4}$$

Since the real-time vale of ε is included in the estimation, improved polarization-nulling can monitor the OSNR accurately regardless of the PMD, nonlinear birefringence, and/or incomplete polarization control. The experiment results are reproduced in Fig 4.2(b), which shows that the OSNR was measured with accuracy better than ±1 dB. The downside of this technique is that it requires multiple receivers and a complicated configuration, making it bulky and expensive.

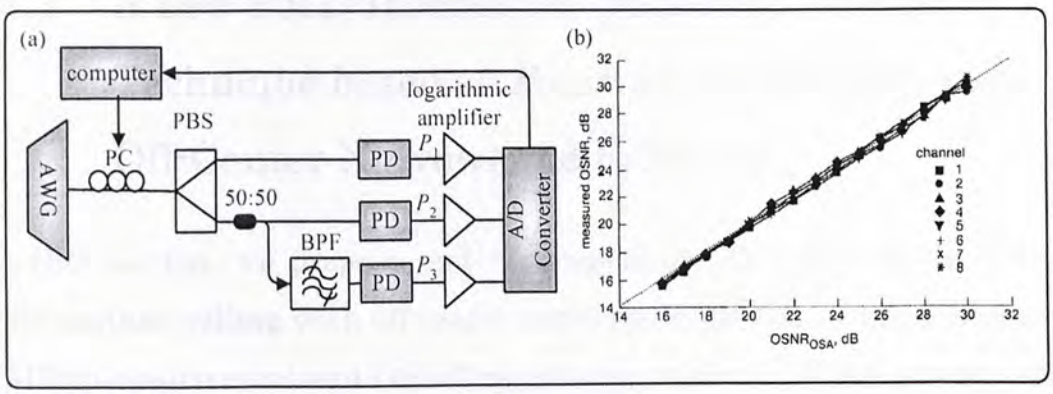

Figure 4.2: (a) Improved polarization-nulling technique (b) OSNR monitoring results by proposed method against that by OSA (Adapted from Ref [71])

4.2.2 Periodic Polarization Encoding Technique

This approach uses periodic polarization encoding of the incoming bit stream to result in spectral nulling of the signal and not the noise in a predesigned wide spectral band, thus allowing extracting the resident OSNR [72]. By replicating the signals with each replica having different amplitude with short and well-defined intervals between the replicas, a finite impulse response filter (FIR) is essentially synthesized. This filter is responsible for setting a predefined spectral region to zero (The spectral response chosen is the Kaiser window because it has a high attenuation ratio in its spectral side lobes) with the ASE noise unaffected. The optical signal is then detected by a photodiode. The analog current produced is passed through a heterodyne mixer and a filter is used to extract the desired spectral band that afterwards is sampled with a narrowband analog-digital (A/D) circuit and processed by a computer. Using this approach, a slightly better monitoring performance against PMD compared with polarization-nulling was obtained. However, this method requires a very complex configuration and precise control.

4.3 A new PMD-Insensitive OSNR Monitoring Technique based on Polarization-Nulling with Off-Center Narrowband Filtering

In this section, we propose and experimentally demonstrate the use of polarization-nulling with off-center narrowband filtering to realize a new PMD-insensitive in-band OSNR monitoring scheme. Unlike conventional polarization-nulling, this scheme uses an off-center narrowband filter to extract a narrowband signal spectrum for nulling to estimate the ASE level [73]. Our proposed scheme is especially suitable for use with signals with a broad spectrum and is thus applicable to 40-Gb/s or even higher data-rate systems using in-band polarization-assisted approach for OSNR monitoring. As an illustration, when applied to a 40-Gb/s 12% RZ-OOK OTDM system with 10-ps and 20-ps DGD, the monitoring errors were reduced from >20 dB to <0.9 dB and <1.6 dB, respectively, demonstrating the promising performance of this scheme even under severe PMD degradation. In addition to its effectiveness, this technique features simplicity, on-the-fly processing, and upgradeability for use in higher data-rate optical systems.

4.3.1 Principle of Proposed Technique

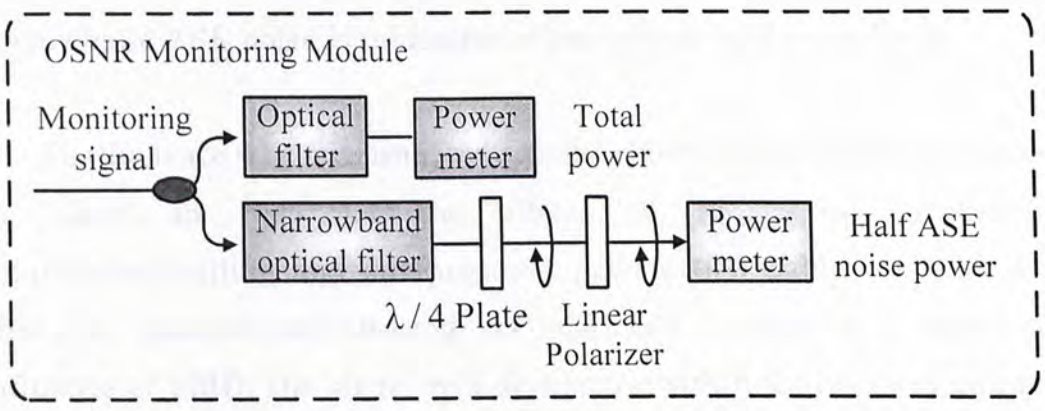

Figure 4.3: Proposed OSNR monitoring module

Fig. 4.3 shows our proposed OSNR monitoring module which consists of two branches: The upper branch consists of a broadband filter to extract the desired optical channel and a power meter to measure the total power P_1 (dBm). The lower branch comprises a narrowband filter positioned at the edge of the signal spectrum, and the signal components extracted are eliminated by a rotating λ/4 plate and linear polarizer, as reported in conventional polarization-nulling [40]. The narrowband noise power, P_2 (dBm), is then measured by a power meter. With P_1 and P_2, we obtain the following:

$$P_{ase}(\text{dBm/0.1nm}) = P_2 + 3 + \alpha_{pol} + \alpha_{\lambda/4} + \alpha_{f2} - 10\log(\frac{NEB_{f2}}{0.1}) \tag{4.5}$$

$$P_{sig}(\text{dBm}) = 10\log[10^{\frac{P_1+\alpha_{f1}}{10}} - (\frac{NEB_{f1}}{0.1})10^{\frac{P_{ase}}{10}}] \tag{4.6}$$

$$OSNR(dB/0.1nm) = P_{sig} - P_{ase} \tag{4.7}$$

where P_{ase} is the ASE noise power referenced to 0.1-nm NEB. The constant 3 doubles the measured ASE noise power since only half of the ASE noise passes through the polarizer. α_{pol}, $\alpha_{\lambda/4}$, α_{f1}, and α_{f2} are the insertion loss of the polarizer, the quarter-wave plate, the broadband filter, and the narrowband filter, respectively. NEB_{f1} and NEB_{f2} are the NEB of

the broadband filter and the narrowband filter, respectively. Our OSNR scheme is based on the assumption that the ASE noise is flat such that the narrowband ASE noise is indicative of the overall ASE noise level.

To illustrate why our proposed scheme shows higher PMD robustness, we show in Fig. 4.4 the effects of PMD on conventional polarization-nulling and our proposed polarization-nulling scheme with off-center narrowband filtering. As explained in chapter 3, under the influence of PMD, the signal will depolarize with a frequency-dependent SOP, causing signal power leakage during noise measurement and vice versa because the polarizer is aligned with a single SOP only. In conventional polarization-nulling, as shown in Fig 4.4(a), the whole depolarized signal spectrum will intrude into the noise measurement, causing very large monitoring errors. On the other hand, our proposed scheme shown in Fig. 4.4(b) exhibits higher PMD robustness due to two factors: (i) we first measure the total power without a polarizer to avoid any underestimation of the total aggregate power of the signal and the ASE; (ii) we use off-center narrowband filtering to extract a fixed portion of ASE and only a small portion of signal for the ASE level estimation. Specifically, "off-center" filtering helps ensure the amplitude of the signal component is small and avert the clock components, while "narrowband" filtering helps ensure the signal extracted has a much confined SOP so that it can be easily filtered out by a polarizer to exclude it in the noise level estimation. In this way, the monitoring errors can be very much reduced.

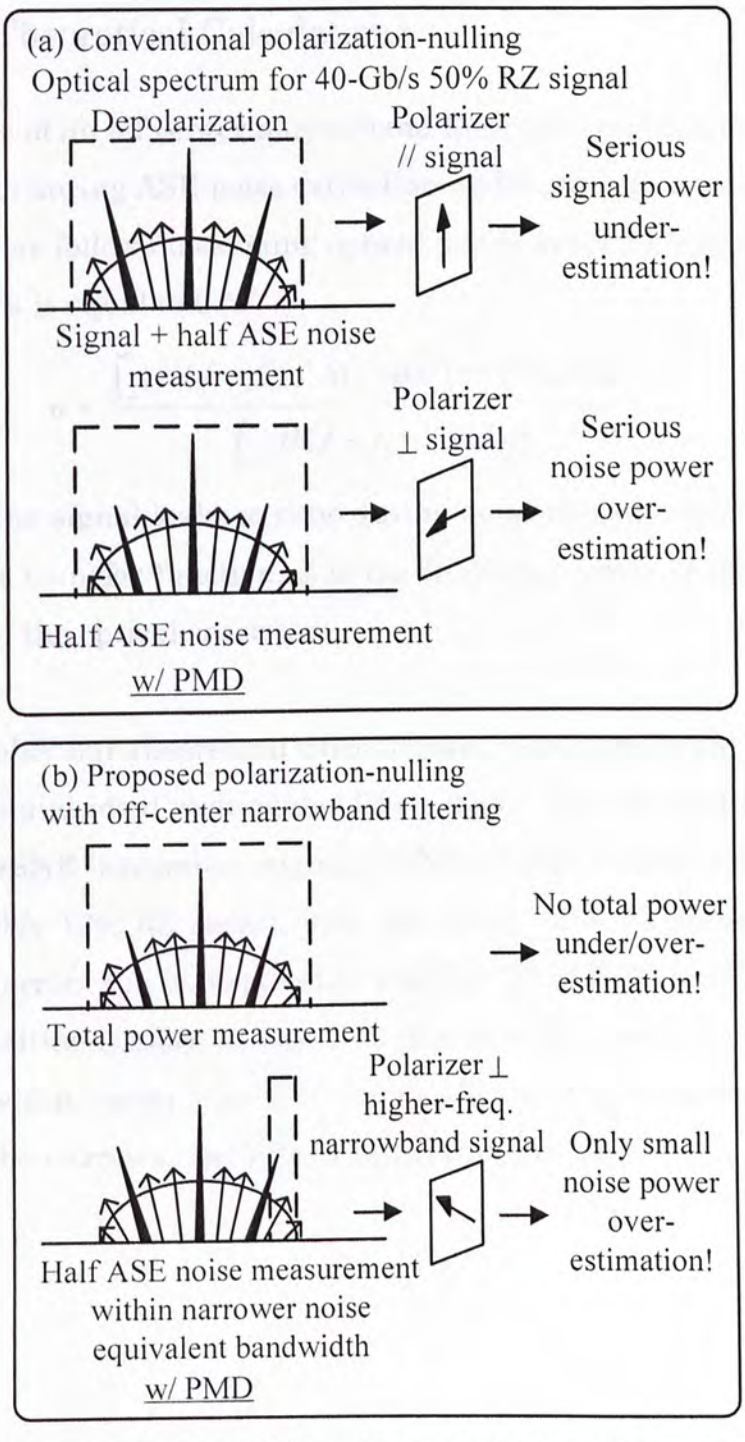

Figure 4.4: Effect of PMD on (a) conventional polari541zation-nulling and (b) polarization-nulling with off-center narrowband filtering

4.3.2 Theoretical Calculations

With the use of an off-center narrowband filter the equation for the signal leakage ratio during ASE noise extraction under the influence of PMD can be modified as follows (assuming optical power splitting ratio, γ, between the two PSPs is equal to 0.5):

$$\alpha = \frac{\int_{-\infty}^{\infty} |H(f-f_0)|^2 \, S(f) \sin^2(\pi * f * DGD) df}{\int_{-\infty}^{\infty} |H(f-f_0)|^2 \, S(f) df} \tag{4.8}$$

where α is the signal leakage ratio during noise measurement, $H(f)$ is the optical filter transfer function, f_0 is the frequency offset of the filter from the center of the optical spectrum.

To simplify our theoretical calculations, we assume ideal rectangular signal pulse and ideal rectangular filter shape. The effect of PMD on the measured OSNR (assuming original OSNR = 25dB/0.1nm) is shown in Fig. 4.6 for 40Gb/s 12% RZ signal, 33% RZ signal, 50% RZ signal, and NRZ signal. The errors can be kept below 2 dB for 10-ps DGD in all cases when the filter position is offset at about 78-85% from the center carrier and the filter bandwidth varies from 0.25 nm to 0.1 nm (The narrower the signal spectrum, the narrower the filter bandwidth to be used).

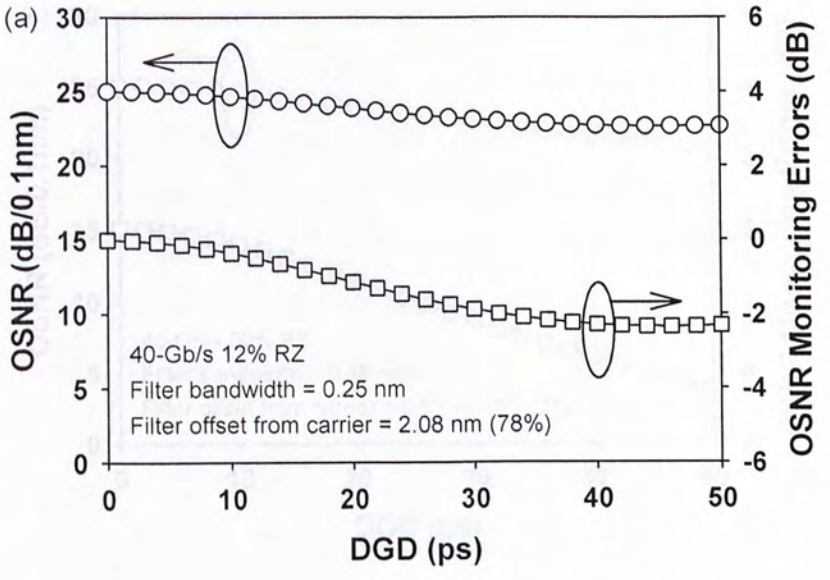
(a)
OSNR (dB/0.1nm)
OSNR Monitoring Errors (dB)
DGD (ps)
40-Gb/s 12% RZ
Filter bandwidth = 0.25 nm
Filter offset from carrier = 2.08 nm (78%)

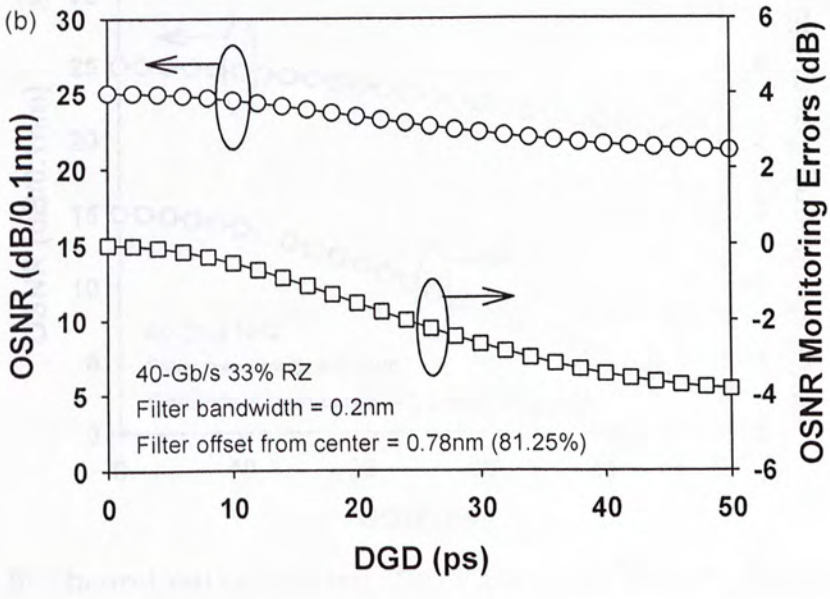
(b)
OSNR (dB/0.1nm)
OSNR Monitoring Errors (dB)
DGD (ps)
40-Gb/s 33% RZ
Filter bandwidth = 0.2nm
Filter offset from center = 0.78nm (81.25%)

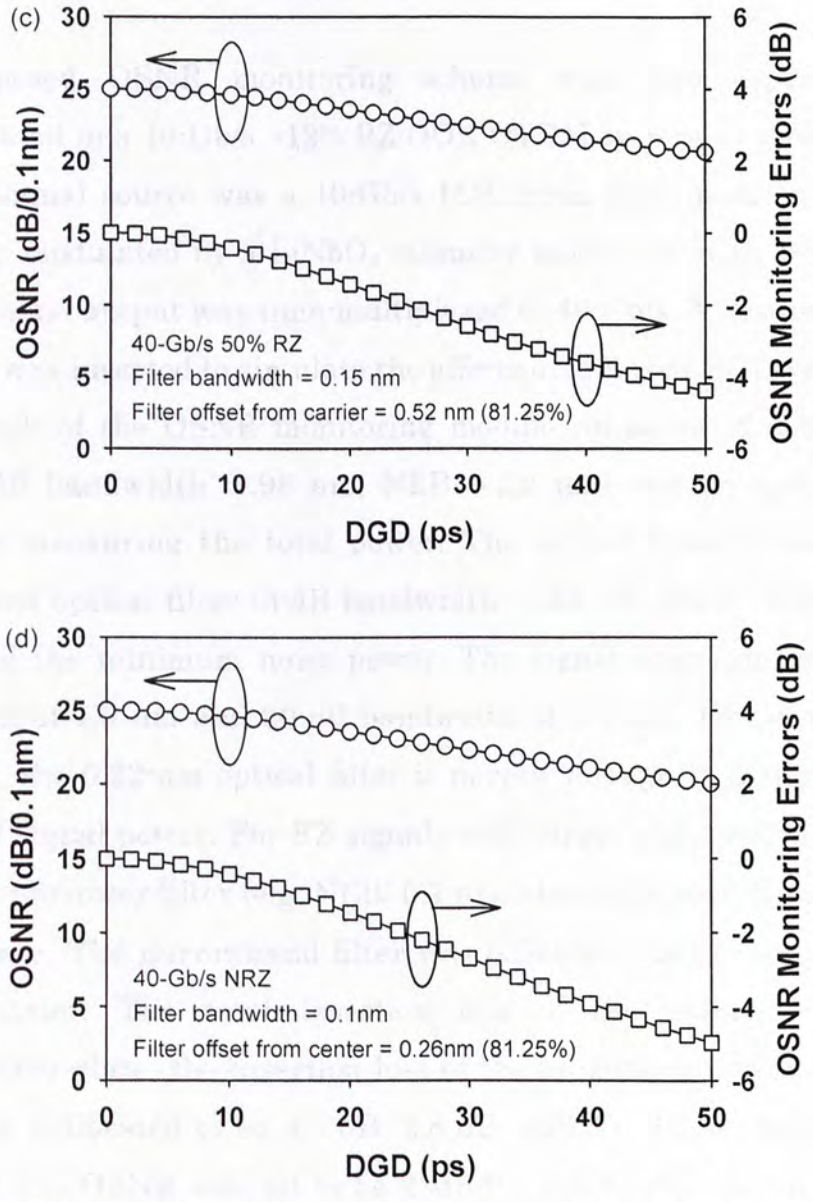

Figure 4.5: Theoretical calculated OSNR (original OSNR: 25dB/0.1nm) for the proposed OSNR monitoring scheme for 40-Gb/s (a) 12% RZ signal, filter bandwidth = 0.25 nm, filter offset from carrier = 2.08 nm (78%), (b) 33% RZ signal, filter bandwidth = 0.2 nm, filter offset from carrier = 0.78 nm (81.25%) (c) 50% RZ signal, filter bandwidth = 0. 15 nm, filter offset from carrier = 0.52 nm (81.25%), and (d) NRZ signal, filter bandwidth = 0.1nm, filter offset from carrier = 0.26 nm (81.25%) under different DGD values

4.3.3 Experimental Results

The proposed OSNR monitoring scheme was also experimentally demonstrated in a 40-Gb/s ~12% RZ-OOK OTDM system as shown in Fig. 4.6. The signal source was a 10-Gb/s 1550.3-nm fiber mode-locked laser externally modulated by a $LiNbO_3$ intensity modulator with 2^{31} -1 PRBS and the signal output was time-multiplexed to 40-Gb/s. A first-order PMD emulator was inserted to simulate the effects of different DGD values. The first branch of the OSNR monitoring module consisted of a broadband filter (3-dB bandwidth: 1.98 nm, NEB: ~2.2 nm) and an optical power meter for measuring the total power. The second branch comprised a narrowband optical filter (3-dB bandwidth: 0.22 nm, NEB: ~0.25 nm) for measuring the minimum noise power. The signal spectrum has a 3-dB bandwidth of 1.6 nm and 20-dB bandwidth of 4.7 nm. For such a broad spectrum, the 0.22-nm optical filter is narrow enough to extract a small portion of signal power. For RZ signals with larger pulse width and NRZ signals, a narrower filter (e.g. NEB: 0.1 nm) should be used to yield better performance. The narrowband filter was offset at 2 nm (~85%) from the center carrier. The total insertion loss of the polarizer and the quarter-wave plate, the insertion loss of the broadband and narrowband filter were calibrated to be 4.5 dB, 2.8 dB, and 5.0 dB, respectively. For reference, the OSNR was set to be 25dB/0.1 nm by the optical spectrum analyzer (OSA). The measurement time for our scheme was within 1 min which was mainly limited by the maximum rotation speed of the quarter-wave plate and could be further improved. However, rotation of SOP during the course of measurement was less a problem because the quarter-wave plate and the polarizer would rotate continuously to search for the minimum power.

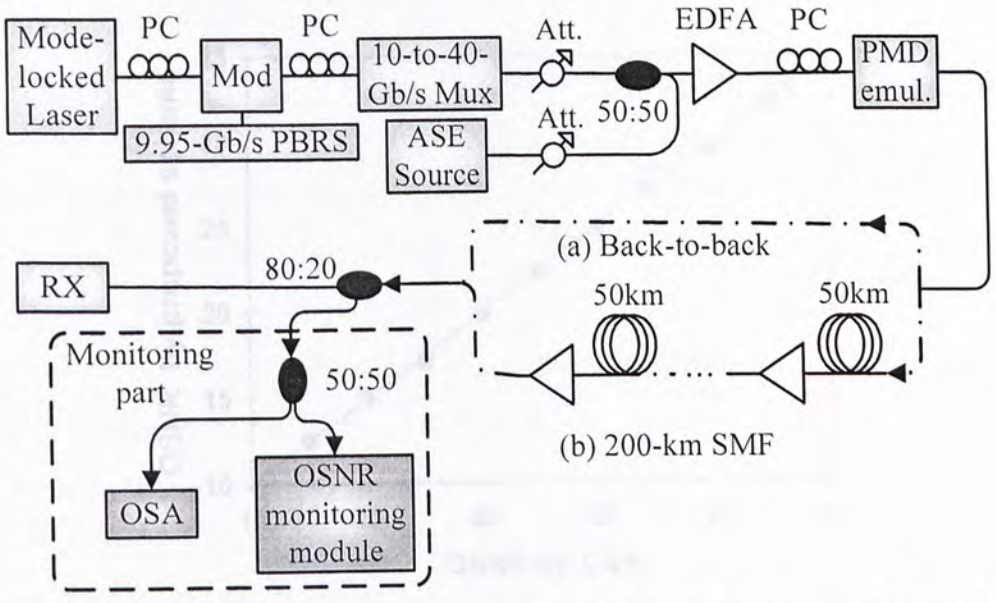

Figure 4.6: Experimental setup to evaluate our proposed scheme: (a) Back-to-back (b) 200-km SMF (total PMD < 1.5 ps)

Fig. 4.7 confirms the OSNR monitoring functionality of our proposed scheme without PMD. The monitoring error was smaller than 0.4 dB for OSNR varying from about 12dB/0.1 nm to 32dB/0.1 nm. Fig. 4.8(a) shows the monitoring errors when DGD is introduced. Without employing off-center narrowband filtering, the absolute monitoring errors increased rapidly with DGD and exceeded 20 dB with only 10-ps DGD. However, with narrowband filtering offset at 2 nm from carrier employed, the monitoring errors were greatly reduced and remained close to zero. This high precision is obtained because the off-center narrowband extracts less than 2% of the total signal power before polarization-nulling and hence the noise can be estimated with a minimum influence of the depolarized signal power when there is PMD.

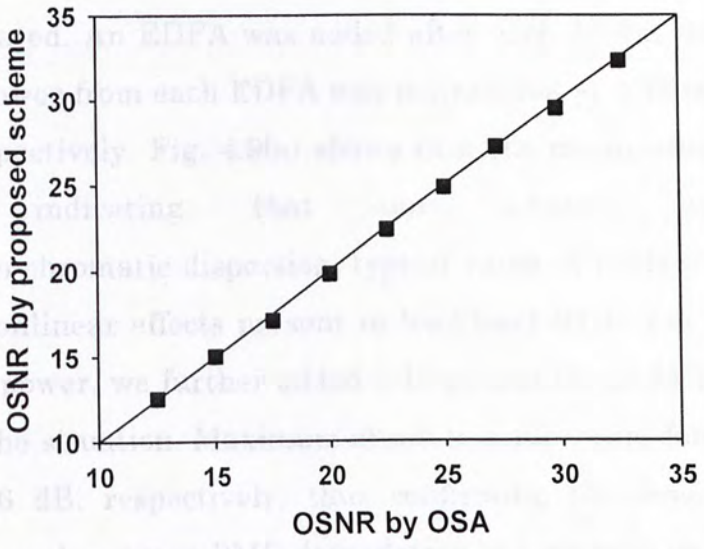

Figure 4.7: OSNR measured by polarization-nulling with off-center narrowband filtering versus OSNR measured by OSA. Monitoring errors <0.4 dB.

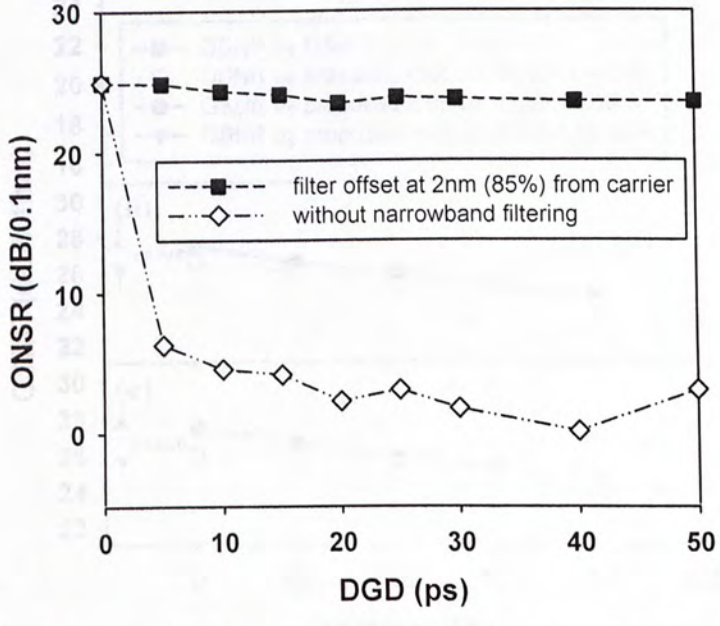

Figure 4.8: Measured OSNR (original: 25dB/0.1nm) with and without employing off-center narrowband filtering at different DGD values

The performance of our scheme after 200-km SMF transmission was also investigated. An EDFA was added after each 50-km SMF span and the output power from each EDFA was maintained at 1 dBm, 5 dBm, and 10 dBm, respectively. Fig. 4.9(a) shows that the monitoring errors were negligible, indicating that our scheme was rather insensitive to chromatic dispersion, typical value of PMD (<1.5 ps in our case), and nonlinear effects present in long-haul SMF. For the case of 1 dBm output power, we further added a 10-ps and 20-ps PMD emulator to exacerbate the situation. Maximum absolute errors were found to be <0.9 dB and <1.6 dB, respectively, thus confirming the feasibility of this scheme even under severe PMD degradation in long-haul transmission.

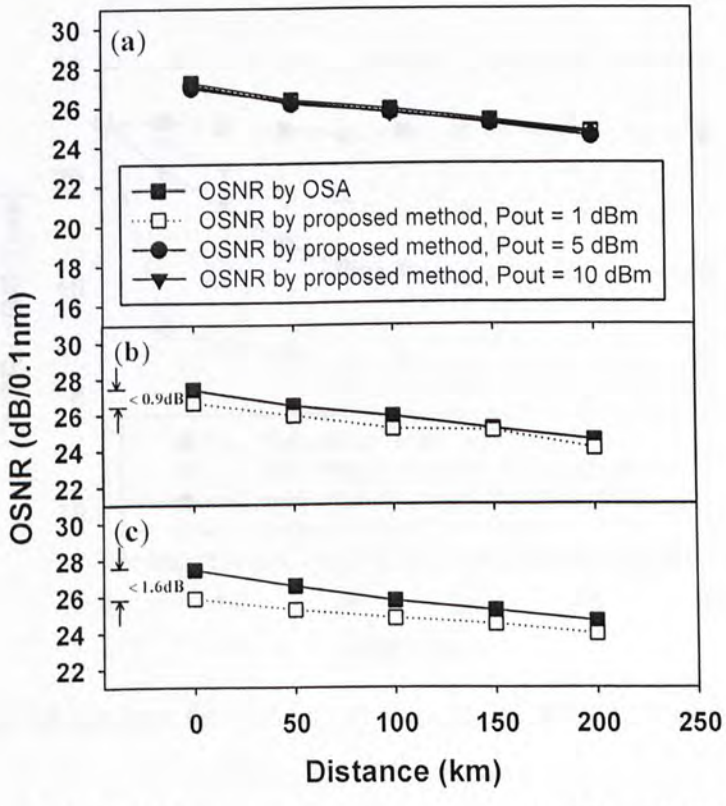

Figure 4.9: OSNR monitoring errors in a 200-km SMF link (a) PMD <1.5 ps, Pout = 1 dBm, 5 dBm, 10 dBm, respectively, (b) with a 10-ps PMD emulator added and Pout = 1 dBm, (c) with a 20-ps PMD emulator added and Pout = 1 dBm.

4.3.4 Effects of Filter Position, Filter Bandwidth, and Filter Detuning

The performance of our proposed scheme was further investigated with the effects of filter position. The experimental setup was the same as in Fig. 4.6 and the filter was offset at 0 nm (without offset), 1 nm, and 2 nm from the carrier and the respective OSNR monitoring errors were measured respectively for different DGD values. The results are shown in Fig 4.10. As expected, the further away the filtering position was from the carrier, the smaller the error was, because the signal components that would intrude into the noise measurements were smaller. Nevertheless a balance was also needed to ensure the filter was kept essentially in-band.

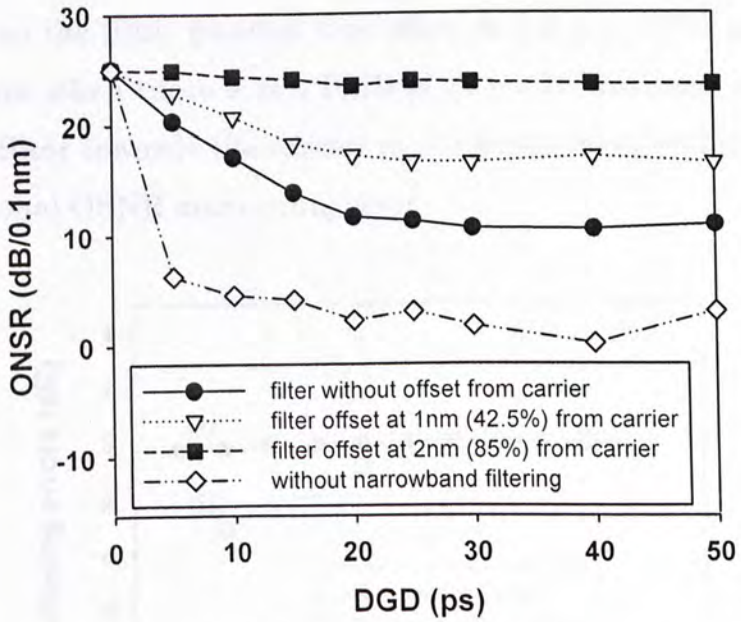

Figure 4.10: Measured OSNR using different filter offset position under different DGD values

Another consideration was the filter bandwidth. A filter with narrower bandwidth could extract signal with much confined SOP but too narrow a filter bandwidth would substantially reduce the output power. In

our experiment, a 0.22-nm filter on 4.7-nm 20-dB bandwidth signal was enough to improve the monitoring performance significantly. Indeed, a compromise was needed between the filter position and filter bandwidth. From our theoretical calculations assuming ideal rectangular pulse and filter shape, a general rule is to use a filter bandwidth of 10% of the modulated signal bandwidth and offset this filter at about 78-85% from the center carrier to obtain <2 dB error (original OSNR: 25dB/0.1nm) at 10-ps DGD.

Since the filter offset position will affect the monitoring accuracy under PMD, we further investigate the effect of filter detuning with a step size of 0.2 nm. The results are shown in Fig. 4.11. It was shown that the errors were negligible when there was no PMD, and could be kept below 2 dB so long as the filter position was offset at 1.8 nm (77%) or more from center carrier when there was a PMD of 10 ps. In this case, a drift of 0.2 nm for the filter towards the carrier in our experiment will cause about a 1-dB additional OSNR monitoring error.

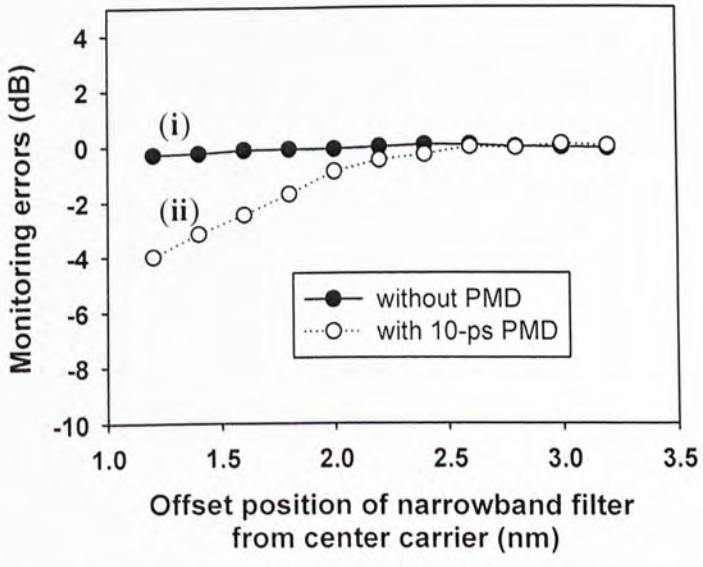

Figure 4.11: Effects of filter detuning (step size: 0.2 nm) for two cases: (i) without PMD, (ii) with 10-ps PMD

4.4 Summary

In this chapter, we have proposed a new and simple OSNR monitoring scheme based on polarization-nulling with off-center narrowband filtering. The off-center narrowband filter helps extract a narrowband signal spectrum for nulling to estimate the ASE level, thus minimizing the influence of the depolarized signal even when there is large PMD. Experimental results demonstrated the excellent performance of this scheme. For instance, with 25dB/0.1nm OSNR set by the OSA and 10-ps DGD, the monitoring error in 40-Gb/s 12% RZ-OOK OTDM system was measured to be >20 dB using conventional polarization-nulling, and was reduced to <0.9 dB by employing narrowband filtering. The proposed technique is simple and easily upgradeable and is expected to be a promising candidate for in-band OSNR monitoring in future networks.

Chapter 5 Simultaneous OSNR and PMD Monitoring using Polarization Techniques

5.1 Introduction

As we have studied in previous chapters, in-band OSNR and PMD are two important parameters to be monitored in high-speed optical networks. In chapter 3, we show that several polarization-assisted approaches to monitor in-band OSNR are significantly affected by the depolarization effect of PMD. In chapter 4, we present several research attempts to decouple the two parameters for accurate in-band OSNR monitoring. The question is that if polarization-assisted methods can monitor OSNR and PMD individually, then why not have them monitor both parameters simultaneously to give a more comprehensive monitoring picture? To date, there has been minimal research done in simultaneously monitor both parameters in a simple manner. In this chapter, we demonstrate that simultaneous OSNR and PMD monitoring can be achieved by using (i) enhanced RF spectral analysis assisted with a local large-DGD element and polarization scrambling at the receiver side, and (ii) DOP-based monitoring with polarization scrambling at the transmitter side.

5.2 Previously Proposed Scheme

A simple simultaneous OSNR and PMD monitoring module based on polarization-nulling assisted by polarization scrambling and orthogonal polarization detection was first proposed in [74] (Fig. 5.1(a)). A PC is

placed in front of the demultiplexer to scramble the polarization state of the incoming monitoring signal. After the demultiplexer, the monitoring signal will be split into two arms using a polarization beam splitter (PBS). In one arm, the monitoring signal is detected directly by a photodiode, electrical amplifier, and a voltmeter. In another arm, the monitoring signal first passes through a BPF with a narrower bandwidth to reduce the ASE noise, and is then detected by a photodiode, electrical amplifier, and a voltmeter. The maximum and minimum voltages of each arm are noted and expressed as follows:

$$V_1^{\max} = G_1[P_s(1-\delta)+0.5P_{ase}] \tag{5.1}$$

$$V_1^{\min} = G_1[P_s\delta+0.5P_{ase}] \tag{5.2}$$

$$V_2^{\max} = G_2[P_s(1-\delta)+0.5\alpha P_{ase}] \tag{5.3}$$

$$V_2^{\min} = G_2[P_s\delta+0.5\alpha P_{ase}] \tag{5.4}$$

where α is the noise power filtering factor of the narrowband filter. The OSNR and depolarization factor can then be obtained by a simple analysis:

$$OSNR = \frac{G_1\overline{V_2}-\alpha G_2\overline{V_1}}{G_2\overline{V_1}-G_1\overline{V_2}} \tag{5.5}$$

$$\delta = \frac{1}{2}[1-\frac{(1-\alpha)(V_1^{\max}-V_1^{\min})}{2(\frac{G_1}{G_2}\overline{V_2}-\alpha\overline{V_1})}] \tag{5.6}$$

The method was reported to be able to monitor OSNR from 18 dB/0.1nm to 36dB/0.1nm and PMD from 0 ps to 70 ps in 10-Gb/s NRZ systems (Fig. 5(b), (c)).

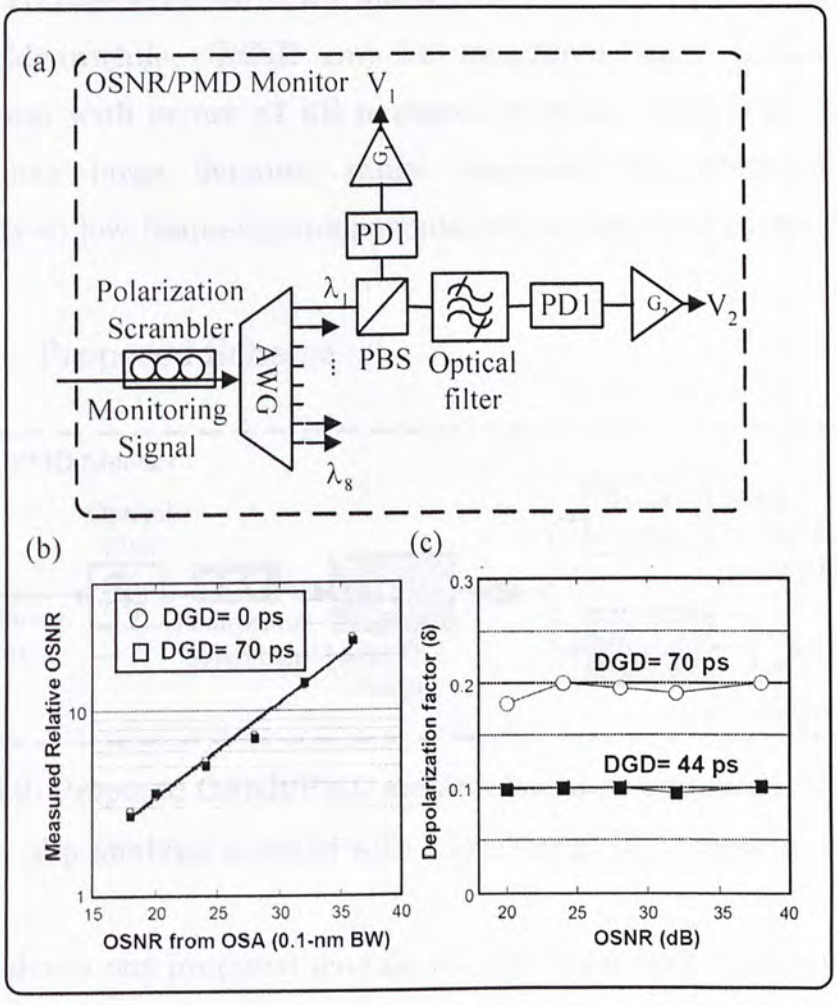

Figure 5.1: (a) Simultaneous OSNR/PMD monitoring module (b) OSNR monitoring results for different PMD (0 ps and 70 ps) (c) PMD monitoring results for different OSNR (Adapted from Ref[74])

5.3 Simultaneous OSNR and PMD Monitoring by Enhanced RF Spectral Analysis

In this section, we report on another technique to simultaneously monitor OSNR and PMD by analyzing the position shift and the minimum power of the RF spectral dip induced by cascading a large-DGD component with polarization scrambling at the monitoring module. Using a 10-Gb/s 3% RZ-OOK system we show that PMD can be monitored from 0 ps to 70 ps

with an average error of ~1.8% (maximum error <5%) irrespective of the OSNR. Meanwhile, OSNR can be monitored from 15dB/0.1nm to 35dB/0.1nm with errors <1 dB irrespective of the PMD. This scheme is simple, has large dynamic range, improves the PMD monitoring sensitivity at low-frequency components, and is potentially low-cost.

5.3.1 Proposed Scheme

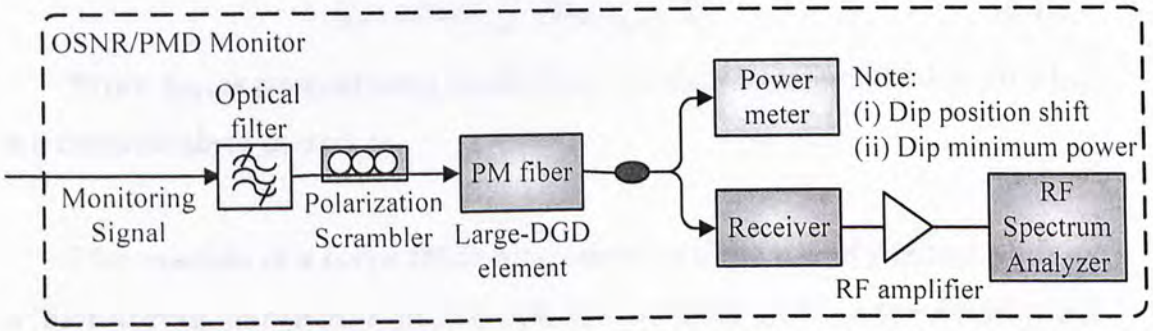

Figure 5.2: Proposed OSNR/PMD monitor based on enhanced RF spectral dip analysis assisted with a local large-DGD element

Fig. 5.2 shows our proposed module for simultaneously monitoring PMD and OSNR. The monitoring signal is sent to an optical filter, a polarization controller (PC) and a piece of polarization maintaining (PM) fiber with a large DGD value. The DGD will generate a dip in the resulting electrical spectrum by destructive interference and the dip frequency is related to the DGD by $f = 1/(2*DGD)$. To monitor PMD, we scramble the PC in front of the PM fiber and note the position shift of the RF spectral dip (i.e. the minimum dip frequency f_{min} and the maximum dip frequency f_{max}) by an RF spectrum analyzer. The principle is as follows: By considering the transmission fiber as one trunk of fiber and the PM fiber in the monitoring module as another, we can express the overall DGD of the cascaded two trunks of fibers as follows [75]:

$$DGD^{2}_{overall} = \beta_1^2 + \beta_2^2 + 2\beta_1\beta_2\cos(\varphi) \qquad (5.7)$$

where β_1, β_2 are the DGD of the two trunks respectively, and φ is the coupling angle between two trunks. From Eqn. (5.7), the maximum and minimum overall DGD can be expressed as:

$$DGD_{\max}^2 = \beta_1^2 + \beta_2^2 + 2\beta_1\beta_2 = (\beta_1 + \beta_2)^2 \tag{5.8}$$

$$DGD_{\min}^2 = \beta_1^2 + \beta_2^2 - 2\beta_1\beta_2 = (\beta_1 - \beta_2)^2 \tag{5.9}$$

Hence, assuming $\beta_1 > \beta_2$,

$$\beta_1 = (DGD_{\max} + DGD_{\min})/2 \tag{5.10}$$

$$\beta_2 = (DGD_{\max} - DGD_{\min})/2 \tag{5.11}$$

Since $f_{\max}$ is proportional to $DGD_{\min}$ and $f_{\min}$ is proportional to $DGD_{\max}$, we can calculate β_1 and β_2.

The cascade of a large-DGD component and the use of position shift as a monitoring parameter in our scheme actually pose some advantages over the previous RF power-based PMD monitoring scheme. In previous scheme, when the transmission link has a small DGD, the RF spectral dip will be at a very high frequency and the power of the low frequency components changes very little, causing low monitoring sensitivity. The cascade of a local large-DGD component can help move the dip position to the low-frequency part of the spectrum even when the transmission link DGD is small. Monitoring at low-frequency components with a higher sensitivity is highly desirable because it not only eliminates the use of high-speed electronics for higher frequency components, but is also insensitive to higher-order PMD [46]. In addition, since the position shift instead of the absolute RF power of the dip is used, our PMD monitoring scheme is strictly dependent on the transmission link DGD and is independent of the signal bit rate. Therefore, no prior knowledge between the RF power level and DGD values is needed.

On the other hand, to monitor OSNR, we note the minimum dip

power during PC scrambling. The minimum power corresponds to the receiver noise power within a narrow resolution bandwidth after signal elimination. This noise power is predominantly the beat noise power which is inversely proportional to the OSNR. The relationship of minimum dip power versus OSNR can be precalibrated for different optical power. We can then estimate the OSNR by measuring the optical power and the receiver noise power, as in orthogonal delayed homodyne method [42]. The presence of PMD may change the dip frequency but the minimum power will remain fairly constant within a considerable PMD range, as explained in chapter 3.

5.3.2 Experimental Results

The proposed monitoring scheme was experimentally demonstrated in a 10-Gb/s 3% RZ-OOK system. A pulse source, generated from a 10-Gb/s 1550.3-nm fiber mode-locked laser, was externally modulated by a $LiNbO_3$ intensity modulator with 2^{31} -1 PRBS. The OSNR was changed by combining the signal with an ASE noise source with different power. A PMD emulator was inserted in the link to simulate different system DGD values. At the receiver side, a small portion (10%) of the signal power was sent to the monitoring module. Due to laboratory availability, the PM fiber used had a DGD of ~409 ps and the nulling frequency was at ~1.22 GHz. In actual deployment, the PM fiber can have a smaller DGD value. Indeed, a tradeoff has to be made when considering the DGD value of the PM fiber. A large-DGD PM fiber can move the spectral dip further to the low frequency part, but the position shift will be smaller for the same transmission link DGD value, resulting in a smaller monitoring sensitivity. A typical DGD value used is 200 ps which produces a dip at 2.5 GHz. In this case, the dip position will change about 50 MHz when the transmission link DGD is only 2 ps.

Fig. 5.3(a)-(b) confirms the PMD and OSNR monitoring functionality of our proposed scheme. The monitoring errors for PMD have an average error of ~1.8% and maximum error <5%, with OSNR varying from 15 dB/0.1nm to 35 dB/0.1nm. On the other hand, the monitoring errors for OSNR were <1 dB, with PMD varying from 0 ps to 70 ps. Fig. 5.4(a) shows the RF spectrum when the PMD emulator was set at 40 ps. The minimum and maximum dip frequency measured was 1.113 GHz and 1.355 GHz, respectively, giving an estimated PMD of 40.1 ps. For OSNR estimation, Fig. 5.4(b) shows the minimum power measurement (=-41.17 dBm) when the OSNR was set at 35dB/0.1nm, giving an estimated OSNR of 34.35dB/0.1nm.

(a)

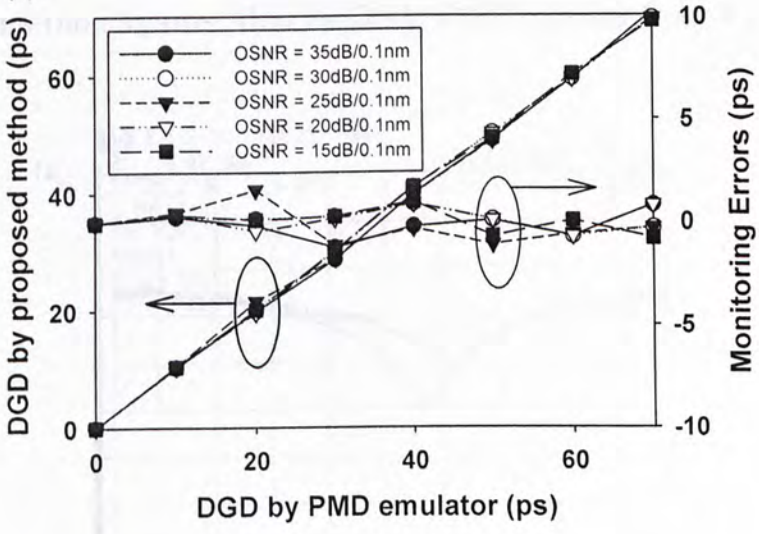

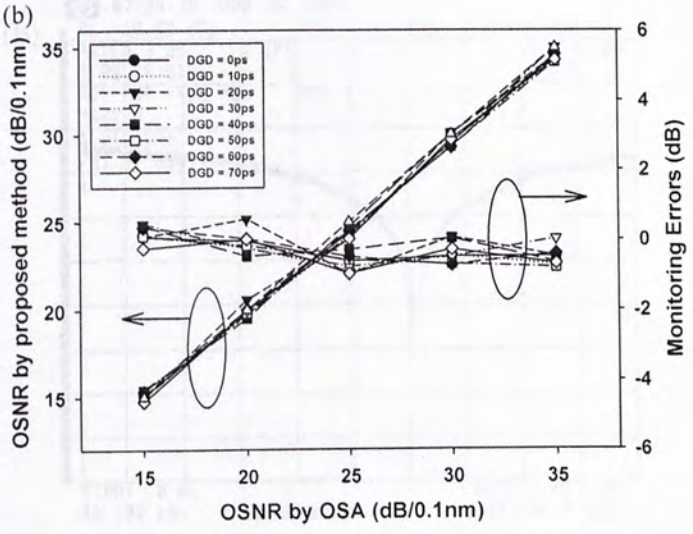

Figure 5.3: (a) PMD monitoring results for 10-Gb/s 3% RZ-OOK by proposed method versus that by PMD emulator, OSNR varying from 15 dB to 35 dB (b) OSNR monitoring results for 10-Gb/s 3% RZ-OOK by proposed method against that by OSA, PMD varying from 0 ps to 70 ps

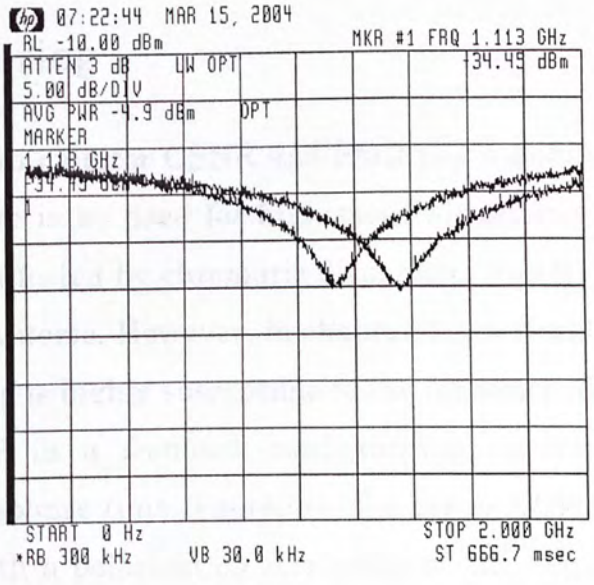

(b)

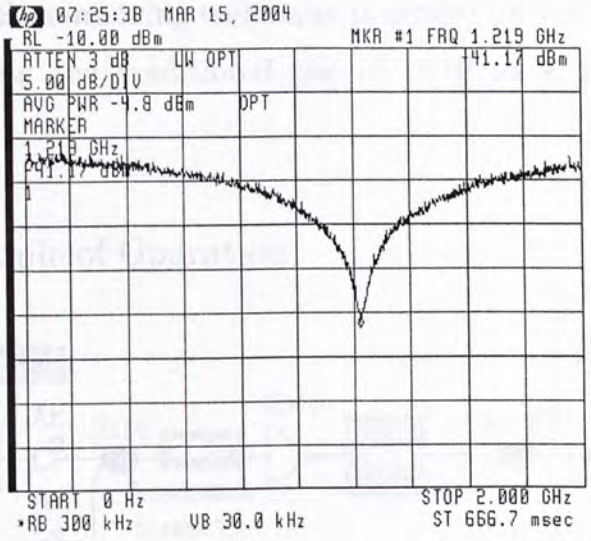

Figure 5.4: (a) RF spectrum showing the position shift of the dip for PMD estimation (b) RF spectrum showing the minimum power of the dip for OSNR estimation

5.4 DOP-based Simultaneous OSNR and PMD Monitoring

The use of DOP to monitor OSNR and PMD has a number of advantages including (i) there is no need for high-speed electronics, (ii) it is simple, and (iii) it is unaffected by chromatic dispersion, and (iv) it is scalable to higher bit-rate systems. However, in chapter 3, we found that DOP-based OSNR monitoring is highly susceptible to the influence of PMD. Moreover, the use of DOP in a feedback configuration requires dithering and decreases the response time. Therefore, the use of DOP in a feed-forward configuration with a polarization scrambler at the transmitter has been proposed [76]-[77]. In this section, we demonstrate that, by putting the PMD monitor in a feed-forward configuration and applying a polarization scrambler at the transmitter side, OSNR and PMD can be simultaneously monitored using a conventional DOP analyzer, thereby making the

DOP-based OSNR monitoring technique practical for use in a real system without sacrificing the traditional use of DOP as a PMD monitoring metric.

5.4.1 Principle of Operation

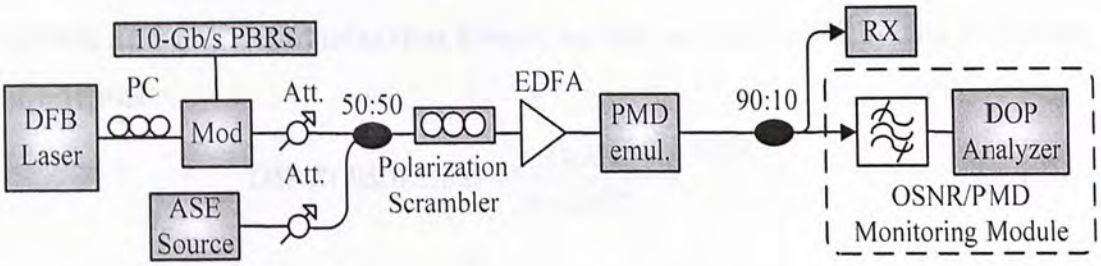

Figure 5.5: Experimental setup for DOP-based simultaneous PMD and OSNR monitoring

Fig 5.5 shows the experimental setup of the DOP-based simultaneous OSNR and PMD monitoring scheme. It consists of a polarization scrambler at the transmitter side and a DOP analyzer preceded by a tunable filter at the receiver side. For OSNR monitoring, a degradation of OSNR will cause a reduction in DOP. It is because an increase in the unpolarized ASE noise power will decrease the ratio of the polarized portion of the total optical power, as explained in chapter 2. For PMD monitoring, the DOP of the received signal is reduced depending on both the DGD and the power splitting ratio, γ, between the two PSPs of the transmission link. The use of the transmitter-side polarization scrambler is to cause the input SOP of the signal to cover the whole Poincare-sphere. When the SOP of the signal is launched at 45° in Jones Space (i.e. $\gamma = 0.5$) with respect to the two PSPs of the transmission link, the DOP measured at the receiver will be minimum. On the other hand, when the SOP of the signal aligns with one of the PSPs (i.e. $\gamma = 0$) of the transmission link, the

DOP measured at the receiver will be maximum, corresponding to the case when there is no effective DGD. Combining the effects of OSNR and PMD together, we can measure the maximum and minimum DOP values at the receiver within one scrambling period to decouple the two effects. The maximum DOP value is dependent on OSNR only, while the minimum DOP value is dependent on both the OSNR and PMD. The OSNR and the depolarization factor, α, can be decoupled by the following equations:

$$OSNR(\text{dB}/0.1\text{nm}) = \left(\frac{DOP_{\max}}{1-DOP_{\max}}\right)\left(\frac{NEB_f}{0.1}\right) \tag{5.12}$$

$$\alpha = DOP_{\min}\left[\left(1+\frac{1}{10^{\frac{OSNR}{10}}}\right)\left(\frac{NEB_f}{0.1}\right)\right] \tag{5.13}$$

where $DOP_{\max}$ and $DOP_{\min}$ are the maximum and minimum DOP measured by the DOP analyzer within the scrambling period, respectively. NEB_f is the noise equivalent bandwidth of the tunable filter before the DOP analyzer. The depolarization factor, α, actually varies from 1 to 0.5 under different DGD in NRZ-OOK systems [46], but the exact *α-DGD* relationship is dependent on the pulse shape and modulator chirp [69]. Thus, to derive DGD from α, a relationship curve has to be calibrated in advance, using signal with an OSNR high enough (i..e. 40dB/0.1nm) such that the ASE noise will cause negligible influence. In this way, simultaneous OSNR and PMD monitoring can be achieved.

5.4.2 Experimental Results

The feasibility of this scheme is demonstrated in a 10-Gb/s NRZ experiment as shown in Fig. 5.5. The monitoring results are shown in Fig. 5.6. It is reported that the scheme can measure PMD from 0 to 80 ps (maximum error <3 ps) irrespective of OSNR and OSNR from 14dB/0.1nm

to 25dB/0.1nm irrespective of PMD (maximum error < 1dB). In Fig 5.6(a), the maximum PMD monitoring error typically occurs in the case of small DGD value because the monitoring sensitivity is lower. In Fig. 5.6(b), as the OSNR gets larger, the maximum DOP approaches one so the errors get larger by Eqn. (5.12). Beyond 25dB/0.1nm OSNR the DOP approaches one and we cannot determine the exact OSNR value but can only say that the OSNR of the signal is >25dB/0.1nm. Fortunately it has been shown in many reports that an OSNR = 25dB/0.1nm is good enough to maintain a BER better than 10^{-9} so it is not necessary to differentiate the higher values of OSNR [30]. On the other hand, when the OSNR falls below 14dB/0.1nm the DOP versus DGD curve will become even flatter when the DGD value is small and has low sensitivity, so the PMD monitoring results will have relatively larger errors.

(a)

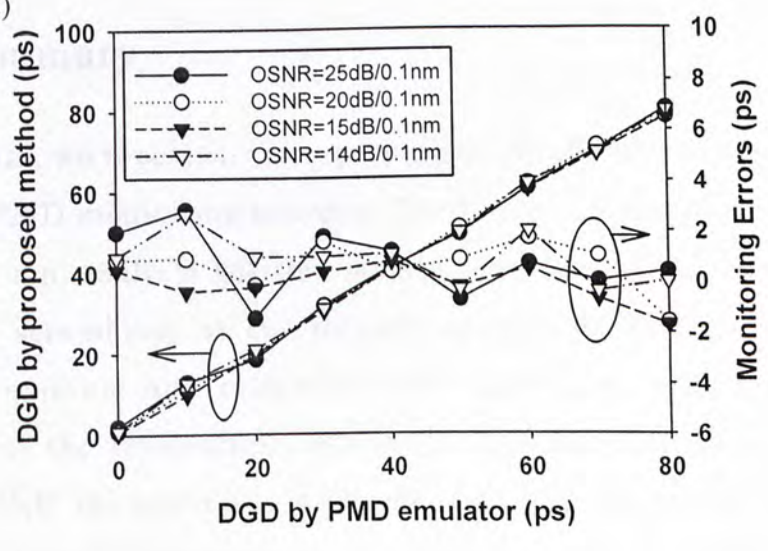

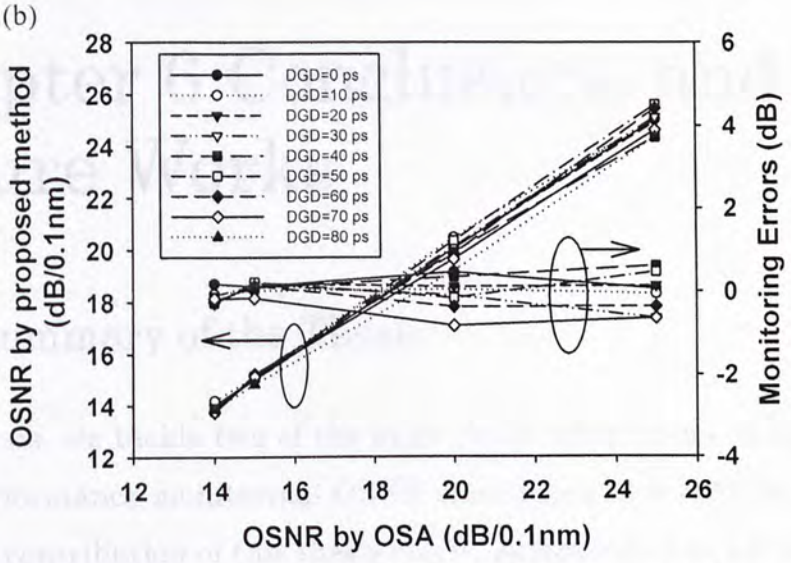

Figure 5.6: (a) PMD monitoring results for 10-Gb/s NRZ signal by proposed method versus that by PMD emulator, OSNR varying from 14 dB to 25 dB (b) OSNR monitoring results for 10-Gb/s NRZ signal by proposed method against that by OSA, PMD varying from 0 ps to 80 ps

5.5 Summary

In this chapter, we report on the experimental results of two simultaneous OSNR and PMD monitoring schemes. The first one is based on enhanced RF spectral dip analysis assisted with a local large-DGD element and polarization scrambling at the monitoring module. The second one is based on maximum and minimum DOP monitoring with polarization scrambling at the transmitter. While the first one has better dynamic range for OSNR, the latter one is not affected by the chromatic dispersion. Experimental results demonstrate the feasibility of both schemes and the information obtained will be important for efficient network management.

Chapter 6 Conclusions and Future Works

6.1 Summary of the Thesis

In this thesis, we tackle two of the most challenging issues in the field of optical performance monitoring: OSNR monitoring and PMD monitoring. The major contribution of this thesis can be summarized as follows:

1. We have provided a detailed quantification of the monitoring errors of in-band polarization assisted OSNR monitoring schemes against DGD for different pulse widths. Our analysis will be valuable for network operators to evaluate whether the schemes are good enough to be deployed based on system conditions.
2. We have proposed and demonstrated a simple PMD-insensitive OSNR monitoring scheme by using two filters of which one is wideband to extract the whole channel and one is narrowband and offset from center carrier to extract the ASE noise with minimum influence of depolarized signal under PMD. When applied to a 40-Gb/s 12% RZ-OOK OTDM system with 10-ps and 20-ps DGD, the monitoring errors were reduced from >20 dB to <0.9 dB and <1.6 dB, respectively. The experimental results demonstrated the promising performance of this scheme even under severe PMD degradation.
3. We have demonstrated two simultaneous OSNR and PMD monitoring techniques with one based on enhanced RF spectral analysis and the other based on DOP. For the first scheme based on the enhanced RF spectrum analysis, using a 10-Gb/s 3% RZ-OOK

system, we showed that PMD could be monitored from 0 ps to 70 ps with an average error of ~1.8% (maximum error <5%) irrespective of the OSNR and OSNR could be monitored from 15dB/0.1nm to 35dB/0.1nm with errors <1 dB irrespective of the PMD. For the second scheme based on DOP analysis, using a 10-Gb/s NRZ system, we showed that PMD could be monitored from 0 to 80 ps (maximum error <3 ps) irrespective of OSNR and OSNR could be monitored from 14dB/0.1nm to 25dB/0.1nm irrespective of PMD (maximum error <1 dB). These two schemes will be attractive candidates for advanced OPM applications of the future.

6.2 Future Works

There are several aspects in which the research can be continued. In our analysis on the robustness of in-band polarization-assisted OSNR monitoring schemes against DGD, we assume that the polarization effect involved is first-order PMD only. The effects of high-order PMD, PDL, and PDG have not been touched upon and further studies concerning these ruinous effects can be carried out. In addition, our study is concerned with NRZ- and RZ-OOK modulation formats only. More analyses on carried suppressed RZ-OOK, alternate-chirped RZ-OOK, and all forms of DPSK formats which attract so much attention recently can be performed.

A common view of the ultimate OPM envisions a simple device that can analyze an optical signal and characterize multiple parameters and a suite of impairments simultaneously. We have demonstrated simultaneous OSNR and PMD monitoring. The most probable next step will be to offer OSNR, PMD, and CD monitoring in a simple monitoring module as there have been many CD monitoring techniques demonstrated which use similar principles to that in PMD monitoring. It is, however, a

great research challenge to decouple one type of impairment in the presence of others in the same time. Additional research effort in this area is surely worthwhile.

Finally, a great challenge ahead is to determine the "right" monitoring information to be collected, i.e. in terms of location, frequency of collecting information, and types of monitoring information. This involves working with higher layer and mathematical optimization. Further research endeavor in this direction will be vital to achieve the most effective deployment of physical layer OPM.

Bibliography

[1] Eugene Park, "Next generation performance monitoring systems for optical metropolitan networks", submitted to *IEEE Communications Magazine*.

[2] Bellcore Generic Requirements GR-253-CORE, Synchronous Optical Network (SONET) Transport Systems: CommonGeneric Criteria.

[3] ITU-T G.957 – Optical Interfaces for Equipments and Systems Relating to the Synchronous Digital Hierarchy, International Telecommunications Union.

[4] ITU-T G.958 – Digital Line Systems Based on the Synchronous Digital Hierarchy for use on Optical Fiber Cables, International Telecommunications Union.

[5] Giammarco Rossi, Timonthy E. Dimmick, and Daniel J. Blumenthal, "Optical performance monitoring in reconfigurable WDM optical networks using subcarrier multiplexing", IEEE *Journal of Lightwave Technology*, vol. 18, no. 12, pp. 1639-1648, December 2000.

[6] Lian Kuan Chen, Man Hong Cheung, Chun Kit Chan, Frank Tong, "Performance monitoring in transparent reconfigurable WDM networks", in *Proc. OECC 2003,* Shanghai, PRC, 2003, Paper 14D1.1.

[7] Alex Vukovic, Michel Savoie, Heng Hua, "Performance monitoring challenges of next generation networks", *Communications Systems and Networks (CSN 2003), IASTED Conference*, Benalmadena, Spain, 2003.

[8] Vinod Ramakrishnan, M. Govindarajan, and John Klonick, "Intelligent performance monitoring in optical networks", *Telecommunications Online*, January 2001.

[9] Abdelhafid Amrani, Jesus Roldan, and Gabriel Junyent, "Optical

monitoring system for scalable all-optical networks", in *Proc. LEOS 1997*, San Francisco, USA, 1997, paper WEE3.

[10] A. Richter, W. Fischler, H. Bock, R. Bach, and W. Grupp, "Optical performance monitoring in transparent and configurable DWDM networks", *IEE Proc.-Optoelectronics*, vol. 149, no. 1, pp. 1-5, February 2002.

[11] Byrav Ramamurthy, Debasish Datta, Helena Feng, Jonathan P. Heritage, and Biswanath Mukherjee, "Impact of transmission impairments on the teletraffic performance of wavelength-routed optical networks", *IEEE Journal of Lightwave Technology*, vol. 17, no. 10, pp. 1713 – 1723, October 1999.

[12] Robert Friskney, Kevin Warbrick, Simon Poliakoff, and Richard Heath, "Link-based photonic path performance prediction and control", in *Proc. ECOC 2002*, Copenhagen, Denmark, 2002, paper 7.4.3.

[13] G. R. Hill, P. J. Chidgey, F. Kaufhold, T. Lynch, O. Sahlen, M. Gustavsson, M. Janson, B. Lagerstrom, G. Grasso, F. Meli, S. Johansson, J. Ingers, L. Fernandez, S. Rotolo, A. Antonielli, S. Tebaldini, E. Vezzoni, R. Gaddedu, N. Caponio, F. Testa, A. Scavennec, M. J. O'Mahony, J. Zhou, A. Yu, W. Sohler, U. Rust, and H. Herrmann, "A transport network layer based on optical network elements", *IEEE Journal of Lightwave Technology*, vol. 11, no. 5/6, pp. 667 – 679, May/June 1993.

[14] William T. Anderson, Janet Jackel, G. -K. Chang, Hongxing Dai, Wei Xin, Matthew Goodman, Chris Allyn, Mario Alvarez, Owen Clarke, Albert Gottlieb, Fred Kleytman, Jay Morreale, Virginia Nichols, Anastasios Tzathas, Ravindra Vora, Linden Mercer, Henry Dardy, Earl Renaud, Leann Williard, James Perreault, Ray McFarland, and Terry Gibbons, "The MONET project – a final report, " *IEEE Journal of Lightwave Technology*, vol. 18, no. 12, pp. 1988 – 2009, December 2000.

[15] Giampaolo Bendelli, Carlo Cavazzoni, Raffaele Girardi, Roberto Lano, "Optical performance monitoring techniques", in *Proc. ECOC 2000*, Munich, Germany, 2000, vol. 4, pp. 113-116.

[16] Richard Habel, Kim Roberts, Alan Solheim, and James Harley, "Optical domain performance monitoring", in *Proc. OFC 2000*, Baltimore, Maryland, 2000, paper WK3-1.

[17] D. C. Kilper, R. Bach, D. J. Blumenthal, D. Einstein, T. Landolsi, L. Ostar, M. Preiss, and A. E. Willner, "Optical performance monitoring", *IEEE Journal of Lightwave Technology*, vol. 22, no. 1, pp. 294 – 304, January 2004.

[18] Richard E. Neuhauser, "Optical performance monitoring (OPM) in next-generation optical networks", APOC 2002, (Invited paper), in *Proc. SPIE 2002*, Shanghai, China, 2002, paper 4909-47.

[19] Q. He, D. Ellis, K. Beckley, R. Maaskant, P. Mock, D. Al-Salameh, Richard DeSalvo, R. McLeod, and W.H. Loh, "Enabling the dynamic enablers: advanced optical performance monitors", in *Proc. LEOS 2002*, Scotland, 2002, paper TuJ4.

[20] Hitoshi Takeshita and Naoya Henmi, "A novel data format free bit-by-bit quasi-error monitoring method for optical transport network" *in Proc. OFC 1999*, San Diego, USA, 1999, paper FJ2-1.

[21] A. L. J. Teixeira, P. S. Andre, M. Lima, J. F. Da Rocha, J. L. Pinto, "Asychronous optical performance monitor techniques for DWDM optical networks", in *Proc. ICTON 2002*, Warsaw, Poland, 2002, paper Mo.A.1.

[22] Dany Yu, and William Yang, "Optical channel performance monitors", *Light Reading*, March 2002.

[23] Tarof L., Performance Monitoring in the Network, *CITO Workshop "Control approaches for optical networks – optimizing the opto-electronics boundaries"*, Ottawa, Canada, December 2002.

[24] Keith Beckley, "Optical performance monitors continue to chase

market", *Lightwave Magazine*, April 2004.

[25] Sava Stanic, Suresh Subramaniam, Hongsik Choi, Gokhan Sahin, and Hyeong-Ah Choi, "On monitoring transparent optical networks", in *Proc ICPPW'02*, Vancouver, Canada, 2002, paper 1530-2016.

[26] J. Strand and A. Chiu, IETF Draft-ieft-ipo-Impairments-05.

[27] TIA/EIA-526-19 standard: OFSTP-19 Optical signal-to-noise ratio measurement procedures for dense wavelength-division systems.

[28] "Optical signal to noise ratio (OSNR)", white paper from Cicadiant Systems Inc., December 2002.

[29] "BER vs. OSNR", white paper from Cicadiant Systems Inc., February 2003.

[30] D. C. Kilper and W. Weingartner, "Monitoring optical network performance degradation due to amplifier noise", IEEE *Journal of Lightwave Technology*, vol. 21, no. 5, pp. 1171-1178, May 2003.

[31] D. C. Kilper, S. Chandrasekhar, L. Buhl, A. Agarwal, and D. Maywar, "Spectral monitoring of OSNR in high-speed networks", in *Proc. ECOC 2002*, Copenhagen, Denmark, 2002, paper p7.4.4.

[32] H. Suzuki and N. Takachio, "Optical signal quality monitor built into WDM linear repeaters using semiconductor arrayed waveguide grating filter monolithically integrated with eight photodiodes", *Electronics Letters*, vol. 35, pp. 836-837, May 1999.

[33] Wenlu Chen, Shan Zhong, Zhonghua Zhu, Wei Chen, and Yung-Jui (Ray) Chen, "Adding OSNR and wavelength monitoring functionalities on a double-resolution-AWG-based power monitoring circuit", *IEEE Photonics Technology Letter*, vol. 15, no. 6, June 2003.

[34] K. Asahi, M. Yamashita, T. Hosoi, K. Nakaya, and C. Konoshi, "Optical performance monitor built into EDFA repeaters for WDM networks", in *Proc. OFC' 98*, San Jose, USA, 1998, paper ThO2.

[35] J. Chappell and S. DeMange, "Optical signal-to-noise ratio characterization demands precision and flexibility", *WDM Solutions*,

vol. 2, no. 6, pp. 55-60, Nov. 2000.

[36] Chun-Liang Yang and San-Liang Lee, "OSNR monitoring using double-pass filtering and dithered tunable reflector", *IEEE Photonics Technology Letters*, vol. 16, no.6, pp.1570-1572, June 2004.

[37] S. K. Shin, K. J. Park, and Y. C. Chung, "A novel optical signal-to-noise-ratio monitoring technique for WDM networks", in *Proc. OFC '2000*, Baltimore, Maryland, 2000, paper WK6.

[38] C. J. Youn, S. K. Shin, K. J. Park, and Y. C. Chung, "OSNR monitoring technique based on high-frequency receiver noise", APOC 2001, in Proc. SPIE 4584, 2001.

[39] M. Rasztovits-Wiech, M. Danner, and W. R. Leeb, "Optical signal-to-noise ratio measurement in WDM networks using polarization extinction", in *ECOC '98*, Madrid, Spain, 1998, pp. 549-550.

[40] J. H. Lee, D. K. Jung, C. H. Kim, and Y. C. Chung, "OSNR monitoring technique using polarization-nulling method", *IEEE Photon. Technol. Lett.*, vol. 13, pp. 88-90, Jan 2001.

[41] Mats Petersson, Henrik Sunnerud, Magnus Karlsson, and Bengt-Erik Olsson, "Performance monitoring in optical networks using stokes parameters", *IEEE Photonics Technology Letters*, vol. 16, no. 2, February 2004.

[42] C. Y. Joun, K. J. Park, J. H. Lee, and Y. C. Chung., "OSNR monitoring technique based on orthogonal delayed-homodyne method", *IEEE Photon. Technol. Lett.*, vol. 14, pp.1469-1471, Oct 2002.

[43] Howard R. Stuart, "Optical performance monitoring using narrowband radio frequency analysis at the half-clock frequency", *Journal of Optical Networking*, vol. 3, no. 6, pp. 396-409, June 2004.

[44] Zhenning Tao, Zhangyuan Chen, Libin Fu, Deming Wu, and Anshi Xu, "Monitoring of OSNR by using a Mach-Zehnder interferometer", Microwave and Optical Technology Letters, vol. 30, no.1, pp. 63-65,

May 2001.

[45] Stephan Wielandy, Michael Fishteyn, and Benyuan Zhu, "Optical performance monitoring using nonlinear detection", IEEE *Journal of Lightwave Technology*, vol. 22, no. 3, pp784-793, March 2004.

[46] A. E. Willner, S. M. R. Motaghian Nezam, L. S. Yan, Z. Pan, and M. C. Hauer, "Monitoring and control of polarization-related impairments in optical fiber systems", *IEEE Journal of Lightwave Technology*, vol. 22, no. 1, pp. 106-125, January 2004.

[47] H. Sunnerud, M. Karlsson, and P. A. Andrekson, "A comparison between NRZ and RZ data formats with respect to PMD-induced system outage probability", *IEEE Photonics Technology Letter*, vol. 13, no. 5, pp. 448-450, May 2001.

[48] H. Bulow, "System outage probability due to first- and second- order PMD", *IEEE Photonics Technology Letter*, vol. 10, no. 5, pp. 696-698, May 1998.

[49] D. Penninckx, F. Roy, S. Lanne, and J. P. Thiery, "Statistical study of dynamic polarization-mode-dispersion compensation based on degree of polarization monitoring", *Microw. Optic. Technol. Lett.*, vol. 25, no. 1, pp. 41-43, May 2000.

[50] Ivan P. Kaminow and Tingye Li, *Optical Fiber Telecommunications IV B Systems and Impairments*, Academic Press, 2002

[51] Q. Yu and A. E. Willner, "Performance limits of first-order PMD compensators using fixed and variable DGD elements", *IEEE Photonics Technology Letter*, vol. 14, no. 3, pp. 304-306, March 2002.

[52] C. Francia, F. Bruyere, J. –P. Thiery, and D. Penninckx, "Simple dynamic polarization mode dispersion compensator", *IEE Electronics Letter*, vol. 35, no. 5, pp. 414-415, March 1999.

[53] S. Bahsoun, J. Negel, and C. Poole, "Measurement of temporal variations in fiber transfer characteristics to 20 GHz due to polarization-mode-dispersion", in *Proc. ECOC'90*, pp. 1003,

postdeadline paper.

[54] F. Heismann, D. A. Fishman, and D. L. Wilson, "Automatic compensation of first order polarization mode dispersion in a 10 Gb/s transmission system", in *Proc. ECOC'98*, vol. 1, pp. 529-530.

[55] H. Y. Pua, K. Peddanarappagari, B. Zhu, C. Allen, K. Demarest, and R. Hui, "An adaptive first-order polarization-mode-dispersion compensation system aided by polarization scrambling: Theory and demonstration", IEEE Journal of Lightwave Technology, vol. 18, no. 6, pp. 832-841, June 2000.

[56] T. Takahashi, T. Imai, and M. Aiki, "Automatic compensation technique for timewise fluctuating polarization mode dispersion in in-line amplifier systems", *IEE Electronics Letter*, vol. 30, no. 4, pp.348-349, February 1994.

[57] G. Ishikawa and H. Ooi, "Polarization-mode-dispersion sensitivity and monitoring in 40-Gb/s OTDM and 10-Gbit/s NRZ transmission experiments" in Proc. OFC'98, Washington, USA, 1998, paper WC5.

[58] S. M. R. Motagian Nezam, Y. W. Song, A. B. Sahin, Z. Pan, and A. E. Willner, "PMD monitoring in WDM systems for NRZ data using a chromatic-dispersion regenerated clock" in Proc. OFC 2002, Anaheim, USA, 2002, pp. 200-202, paper WE5.

[59] M. Hayashi, H. Tanaka, and M. Suzuki, "Low frequency band monitoring method for PMD compensation", IEE Electronics Letter, vol. 38, no. 24, pp.1564-1565, November 2002.

[60] D. Sandel, M. Yoshida-Dierolf, R. Noe, A. Schopflin, E. Gottwald, and G. Fischer, "Automatic polarization mode dispersion compensation in 40Gb/s optical transmission systems, " *IEE Electronics Letter*, vol. 34, no. 23, pp. 2258-2259, Nov. 1998.

[61] S. M. R. Motaghian Nezam, Y. Wang, M. Hauer, S. Lee, and A. E. Willner, "Simultaneous PMD monitoring of several WDM channels using subcarrier tones", in *Proc. CLEO 2001*, Baltimore, Maryland,

2001, pp. 561-563, paper CFE1.

[62] F. Buchali, S. Lanne, J. –P. Thiery, W. Baumert, and H. Bulow, "Fast eye monitor for 10 Gbit/s and its application for optical PMD compensation", in *Proc. OFC 2001*, Anaheim, USA, 2001, TuP5-1/TuP5-3.

[63] F. Buchali, W. Baumert, H. Bulow, and J. Poirrier, "A 40 Gb/s eye monitor and its application to adaptive PMD compensation", in *Proc. OFC 2002*, Anaheim, USA, 2001, pp. 202-203, paper WE6.

[64] B. W. Hakki, "Polarization mode dispersion compensation by phase diversity detection", *IEEE Photonics Technology Letters*, vol. 9, no. 1, January 1997.

[65] R. Noe, D. Sandel, V. Mirvoda, F. Wust, and S. Hinz, "Polarization mode dispersion detected by arrival measurement of polarization-scrambled light", *IEEE Journal of Lightwave Technology*, vol. 20, no. 2, February 2002.

[66] Nobuhiko Kikuchi, "Analysis of signal degree of polarization degradation used as control signal for optical polarization mode dispersion compensation", *IEEE Journal of Lightwave Technology*, vol. 19, no. 4, April 2001.

[67] S. M. R. Motaghian Nezam, A. Sahin, J. McGeehan, Z. Pan, T. Luo, Y. Song, "Polarization state rotation filtering for single sideband generation and carrier suppression using a variable dgd element", in *Proc. OFC 2003*, Atlanta, USA, 2003, paper FM7.

[68] S. M. Reza Motaghian Nezam, John E. McGeehan, and Alan E. Willner, "Theoretical and experimental analysis of the dependence of a signal's degree of polarization on the optical data spectrum", *Journal of Lightwave Technology*, vol. 22, no. 3, pp.763-772, March 2004

[69] Nobuhiko Kikuchi, "Analysis of signal degree of polarization degradation used as control signal for optical polarization mode dispersion compensation", *IEEE Journal of Lightwave Technology*, vol.

19, no. 4, pp. 480-486, April 2001.

[70] Govind P. Agrawal, *Nonlinear Fiber Optics*, 3rd edition, Academic Press, 2001.

[71] J. H. Lee and Y. C. Chung, "Improved OSNR monitoring technique based on polarization-nulling method", *IEE Electronics Letter*, vol. 37, no.15, pp. 972 – 973, July 2001.

[72] Z. Zalevsky, D. Abraham, V. Eckhouse, and Y. Beiderman, "In-band optical signal-to-noise ratio network monitoring using periodic polarization modulation", *Journal of Optical Networking*, vol. 2, pp. 303-314, Sept 2003.

[73] M. H. Cheung, L. K. Chen, and C. K. Chan, "A PMD-insensitive OSNR monitoring scheme based on polarization-nulling with off-center narrowband filtering", in *Proc. OFC 2004*, Los Angeles, CA, 2004, paper FF2.

[74] L. S. Yan, Y. Q. Shi, X. Steve Yao, and A. E. Willner, "Simultaneous montioring of both OSNR and PMD using polarization techniques", in *Proc. ECOC'03*, Rimini, Italy, 2003, paper We4.P.133.

[75] M. Wegmuller, S. Demma, C. Vinegoni, and N. Gisin, "Emulator of first- and second-order polarization-mode disperision", *IEEE Photonics Technology Letter*, vol. 14, no.5, pp. 630-632, May 2002.

[76] H. Rosenfeldt, Ch. Knothe, R. Ulrich, E. Brinkmeyer, U. Feiste, C. Schubert, J. Berger, R. Ludwig, H. G. Weber, A. Ehrhardt, "Automatic PMD compensation at 40 Gbit/s and 80 Gbit/s using a 3-dimensional DOP evaluation for feedback", in *Proc. OFC 2001*, Anaheim, USA, 2001, paper PD27-1-PD27-3.

[77] H. Rosenfeldt, R. Ulrich, E. Brinkmeyer, U. Feiste, C. Schubert, J. Berger, R. Ludwig, H. G. Weber, A. Ehrhardt, "Feed-forward approach for automatic PMD-compensation at 80 Gbit/s over 45 km installed single mode fiber", in *Proc. ECOC 2001*, Amsterdam, the Netherlands, vol.6, pp.68-69, paper PD.B.1.1.

Appendix – List of publications

1. Lian-Kuan Chen, Man-Hong Cheung, Chun-Kit Chan, Frank Tong, "Performance monitoring in transparent reconfigurable WDM networks", in *Proc. OECC 2003*, Shanghai, PRC, 2003, Paper 14D1.1 (Invited paper).

2. Man-Hong Cheung, Lian-Kuan Chen, Chun-Kit Chan, "On robustness of in-band polarization-assisted OSNR monitoring schemes against PMD", in *Proc. CLEO/PR 2003*, Taipei, Taiwan, 2003, Paper W1J.

3. Man-Hong Cheung, Lian-Kuan Chen, Chun-Kit Chan, "A PMD-insensitive OSNR monitoring scheme based on polarization-nulling with off-center narrowband filtering", in *OFC 2004*, Los Angeles, USA, paper FF2.

4. Guo-Wei Lu, Man-Hong Cheung, Lian-Kuan Chen, Chun-Kit Chan, "Simultaneous PMD and OSNR monitoring by enhanced RF spectral dip analysis assisted with a local large-DGD element", to appear in *Proc. ECOC 2004*, Stockholm, Sweden, Paper We4.P.

5. Man-Hong Cheung, Lian-Kuan Chen, Chun-Kit Chan, "PMD-insensitive OSNR monitoring based on polarization-nulling with off-center narrowband filtering", to appear in *IEEE Photonics Technology Letter*, vol. 16, no. 11, Nov 2004.